



Originally published as:

Heinrich, I., Touchan, R., Dorado Liñán, I., Vos, H., Helle, G. (2013): Winter-to-spring temperature dynamics in Turkey derived from tree rings since AD 1125. - *Climate Dynamics*, 41, 7-8, 1685-1701

DOI: [10.1007/s00382-013-1702-3](https://doi.org/10.1007/s00382-013-1702-3)

1 **Winter-to-spring temperature dynamics in Turkey derived from tree rings since**
2 **AD1125**

3

4 Ingo Heinrich^{1*}, Ramzi Touchan², Isabel Dorado Liñán¹, Heinz Vos³, Gerhard Helle¹

5

6 ¹ *Helmholtz Centre Potsdam, GFZ German Research Centre for Geosciences, Telegrafenberg,*
7 *14473 Potsdam, Germany*

8 ² *Laboratory of Tree-Ring Research, University of Arizona, Tucson, USA*

9 ³ *Forschungszentrum Jülich, Institute for Chemistry and Dynamics of the Geosphere,*

10 *Wilhelm-Johnen-Str., 52425 Jülich, Germany*

11

12 * Corresponding author:

13 Helmholtz Centre Potsdam, GFZ German Research Centre for Geosciences,

14 Climate Dynamics and Landscape Evolution, Telegrafenberg, 14473 Potsdam, Germany

15 Tel.: +49 331 288 1915; fax: +49 331 288 1302

16 *E-mail address:* heinrich@gfz-potsdam.de

17

18 **Abstract**

19 In the eastern Mediterranean in general and in Turkey in particular, temperature
20 reconstructions based on tree rings have not been achieved so far. Furthermore, centennial-
21 long chronologies of stable isotopes are generally also missing. Recent studies have identified
22 the tree species *Juniperus excelsa* as one of the most promising tree species in Turkey for
23 developing long climate sensitive stable carbon isotope chronologies because this species is
24 long-living and thus has the ability to capture low-frequency climate signals. We were able to

25 develop a statistically robust, precisely dated and annually resolved chronology back to
26 AD1125. We proved that variability of $\delta^{13}\text{C}$ in tree rings of *J. excelsa* is mainly dependent on
27 winter-to-spring temperatures (January to May). Low-frequency trends, which were
28 associated with the medieval warm period and the little ice age, were identified in the winter-
29 to-spring temperature reconstruction, however, the 20th century warming trend found
30 elsewhere could not be identified in our proxy record, nor was it found in the corresponding
31 meteorological data used for our study. Comparisons with other northern-hemispherical proxy
32 data showed that similar low-frequency signals are present until the beginning of the 20th
33 century when the other proxies derived from further north indicate a significant warming
34 while the winter-to-spring temperature proxy from SW-Turkey does not. Correlation analyses
35 including our temperature reconstruction and seven well-known climate indices suggest that
36 various atmospheric oscillation patterns are capable of influencing the temperature variations
37 in SW-Turkey.

38

39 *Keywords:* tree rings; *Juniperus excelsa*; temperature reconstruction; stable carbon isotopes; $\delta^{13}\text{C}$;
40 climate indices

41

42 **1 Introduction**

43 The climate of the eastern Mediterranean is characterised by extremes of heat, highly variable
44 precipitation, and limited water resources. These features are of great significance to the
45 growing human populations and can play a role in the dynamics of regional demographic,
46 socio-cultural, economic, and environmental changes of the area (Türkeş 1998). Therefore,
47 understanding natural climate variability is of great importance as it will help to better predict
48 its future variability, thus helping the societies affected to better adapt to the effects of climate
49 change. Developing this understanding is difficult from the relatively short instrumental

50 record available for the eastern Mediterranean region (Türkeş and Erlat 2003). Gassner et al.
51 (1942) already remarked that for most parts of Turkey meteorological data were collected
52 only since the late 1920s. Alternatively, natural archives such as tree rings and other proxy
53 records can be used to capture information about climate variability on longer time scales.
54 Tree rings are unique in their ability to provide high-resolution, absolutely dated climate
55 signals for the study of palaeoclimatology (Hughes et al. 2010).

56 Stable carbon isotopes in tree rings are valuable sources for studies on climate
57 reconstructions. The variability of isotope records from tree rings is closely dependent on the
58 impact of environmental changes on plant physiological processes, mainly photosynthesis and
59 transpiration. During the vegetation period signals from plant ecophysiological processes are
60 integrated over time into the individual tree rings. The use of stable carbon isotopes from
61 plant organic material as a palaeoclimate proxy is based on a model which considers the
62 fractionation of the stable carbon isotopes during photosynthetic uptake of CO₂ in the leaves.
63 The degree of fractionation depends on the rate of stomatal conductance and the rate of
64 photosynthesis, which are influenced by a number of direct and indirect factors such as the
65 environmental factors precipitation and temperature (e.g., McCarroll and Loader 2004).

66 So far only a few dendroclimatological studies have been conducted in Turkey (Gassner et al.
67 1942; Akkemik 2000, 2003; D'Arrigo and Cullen, 2001; Hughes et al. 2001; Touchan et al.,
68 2003, 2005; Akkemik and Aras, 2005; Griggs et al. 2007; Sevgi and Akkemik 2007; Touchan
69 et al. 2007; Akkemik et al. 2005, 2008; Köse et al. 2011). Gassner et al. (1942) identified
70 winter and spring precipitation as the major growth limiting factor while temperature did not
71 play an important role in central Turkey. Akkemik (2000) determined the relationship
72 between tree rings of *Pinus pinea* from the Istanbul region and temperature and precipitation
73 data. He found a significant positive correlation with summer precipitation and a weak
74 positive correlation with spring temperature. D'Arrigo and Cullen (2001) reconstructed
75 precipitation back to AD 1628 for central Turkey based on five tree-ring chronologies. The

76 reconstruction showed some correspondences with the Euphrates River streamflow and the
77 North Atlantic Oscillation. Akkemik (2003) carried out a calibration study focusing on tree
78 rings of *Cedrus libani* at the northern boundary of its natural distribution in northern Turkey.
79 The response functions analysis suggested positive correlation between ring widths and
80 winter-to-spring temperature and spring-to-summer precipitation. A reconstruction of spring
81 precipitation back to AD 1635 using oak tree rings in the western Black Sea region of Turkey
82 corroborated historical records of droughts in Turkey (Akkemik et al. 2005). Touchan et al.
83 (2003, 2007) developed May-to-June precipitation reconstructions for southwestern Turkey
84 based on tree rings of Cedar, Juniper and two Pine species. The reconstructions showed clear
85 evidence of multi-year to decadal variations in spring precipitation. Additional analyses of
86 links between large-scale climatic variation and these climate reconstructions showed some
87 relationships between extremes in spring precipitation and anomalous atmospheric circulation
88 in the region. However, the relationships between major European-scale circulation patterns
89 and the reconstructed May-to-June precipitation was insignificant which suggested that more
90 local factors and processes have mainly been influencing tree-ring variability over the last
91 centuries (Touchan et al. 2005). Akkemik and Aras (2005) studied tree rings of *Pinus nigra*
92 and developed a reconstruction of summer precipitation for southern Central Turkey back to
93 AD 1689. Although the authors could identify a significant negative correlation between the
94 North Atlantic oscillation and instrumental precipitation data, the correlation was lower and
95 non-significant between the reconstructed precipitation and NAO. Griggs et al. (2007) found
96 that May-to-June precipitation is the primary limiting factor in annual tree-ring growth of
97 oaks of northeastern Greece and northwestern Turkey. Making use of this relationship the
98 authors calculated a regional reconstruction of May-to-June precipitation for AD 1089-1989.
99 The mean May-to-June temperature was also shown to be a growth-limiting factor indicated
100 by a significant negative correlation. In tree-ring reconstructions of spring-summer
101 precipitation and streamflow for north-western Turkey, which both emphasize high-frequency

102 variations, Akkemik et al. (2008) were able to identify common climatic extremes back to AD
103 1650 over much of the country. In a dendroecological study of *Pinus nigra* at different
104 altitudes in Kazdaglari, NW Turkey, Sevgi and Akkemik (2007) showed varying and unclear
105 correlations between tree rings and climate. Precipitation was often positively correlated with
106 tree rings in summer and temperature was positively correlated with tree rings either in winter
107 or in spring-to-summer depending on the altitude.

108 Recently, Köse et al. (2011) reconstructed May–June precipitation for western Turkey by
109 means of tree rings of *Pinus nigra*. The reconstruction contained mostly short drought events
110 with the longest consecutive dry period between 1925 and 1928. The comparison with
111 historical data of agricultural famine years suggested a close relationship to such dry years as
112 determined from the reconstruction. Hughes et al. (2001), making use of a large
113 archaeological dataset, conducted an extreme year analysis of a multi-millennial master tree-
114 ring chronology for the Aegean region consisting mainly of archaeological wooden objects.
115 They showed that the so-called pointer years were associated with circulation anomalies
116 responsible for precipitation-bearing systems influencing the region in springtime.

117 The review of the studies conducted in Turkey so far has shown that several tree species have
118 been investigated for their climate responses. The tree-ring series of most species seem to
119 correlate best with precipitation and to some extent with temperature. However, the tree-ring
120 studies were always based on ring-width measurements and always resulted in reconstructions
121 of precipitation and drought indices. Studies of tree-ring based temperature reconstructions
122 and stable isotopes in tree rings are, to our knowledge, still lacking in Turkey.

123 The aim of this paper is to present a first multi-centennial stable carbon isotope chronology
124 derived from tree rings of *Juniperus excelsa* M. Bieb. trees from a mountainous site near
125 Antalya, Turkey. Since this is the first tree-ring isotope record from Turkey, its usefulness for
126 further palaeoclimatology is evaluated. We analyze its response to climate and reconstruct the
127 selected climate variable. Since stable isotope series do not have age trend problems such as

128 ring width measurements (McCarroll and Loader 2004; Gagen et al. 2006; Treydte et al.
129 2006), statistical *a-priori* filtering will not be necessary and hence it can be expected that
130 high- and low-frequency climate signals will be retrieved from the isotope record.

131 Moreover, the study investigates the spatial and temporal correlation patterns of the climate
132 growth relationships in order to assess the stability, i.e., quality of this new climate
133 reconstruction in Turkey. It also aims to examine possible climate trends found similarly in
134 our and other reconstructions derived from already existing proxy records and to assess if
135 extremely cold or hot years indicated by our record are corroborated by historical
136 documentary data.

137 Finally, temporal correlations calculated between the new climate proxy and various climate
138 indices established for geographical regions surrounding Turkey (e.g., NAO, MOI, NINO4,
139 etc.) are presented to help understand the climate dynamics in Turkey. The eastern
140 Mediterranean is influenced by some of the most relevant mechanisms acting upon the global
141 climate system. It lies in a transitional zone between the arid zone of the subtropical high of
142 North Africa and the temperate zone of central and northern Europe affected by westerly
143 flows. Several studies (Conte et al. 1989; Kutiel and Maheras 1998; Kadioglu et al. 1999;
144 Kutiel and Benaroch 2002; Kutiel et al. 2002; Xoplaki 2002; Kutiel and Türkeş 2005; Türkeş
145 and Erlat 2008, 2009) examined the temperature regime over the Eastern Mediterranean basin
146 and the relationship between temperature variations and circulation indices in order to identify
147 those indices that have the strongest influence on the temperature variations. The
148 Mediterranean climate seems to be influenced by the South Asian Monsoon in summer, the
149 Siberian High Pressure System in winter, and the El Niño Southern Oscillation (ENSO) and
150 the North Atlantic Oscillation (NAO) throughout the year (e.g., Corte-Real et al. 1995;
151 Maheras et al. 2000; Ribera et al. 2000).

152

153 **2 Materials and methods**

154 2.1 Study site

155 The study site Jsibeli (36°36'N / 30°01'E) is located near Elmali in the Antalya district of
156 southwest Turkey at an elevation of 1850 to 2020 m above sea level (Fig. 1). The site is
157 situated on the southwest slopes of the Taurus Mountains, which divide the Mediterranean
158 coastal region from the central Anatolian Plateau. Based on the classification by Türkeş
159 (1998) and Türkeş et al. (2002) Turkey has four major rainfall regions. Jsibeli is situated in
160 the Mediterranean climate region (MED) which is characterized by dry, hot summers and
161 cool, rainy winters (Türkeş 1996; Türkeş et al. 2002). In the MED region, precipitation
162 follows a strong seasonal pattern, with most of the precipitation occurring during the cold
163 season and small amounts during summer. The total annual precipitation is approximately 750
164 mm and the wintertime is characterized by a water surplus while the warmer seasons by a
165 water deficit. The summer dryness is often associated with large-scale regional climate that is
166 controlled by both mid-latitude (more European climate) and North African-Asiatic tropical
167 (*e.g.*, monsoon low) pressure systems (Türkeş and Erlat 2003). Due to the relatively high
168 altitude (1850-2020m a.s.l.), the site is covered with snow from December-to-April (Türkeş et
169 al. 2002). The mean annual temperature ranges from 10.1°C to 13.2°C. July is the warmest
170 month, with an average temperature between 20.3°C and 25.9°C. January is the coldest
171 month, with an average temperature ranging from -4.9°C to 5.9°C (Turkish General
172 Directorate of Meteorology 2008).

173 The site at Jsibeli is a pure *Juniperus excelsa* open forest stand with trees several hundred
174 years old. This type of forest can be regarded as remnant after the Beyşehir occupation
175 clearance phase which took place between 1250BC to AD800. Before this period southwest
176 Turkey had been covered by various species of the genera *Cedrus*, *Pinus*, *Abies*, *Juniperus*
177 and deciduous *Quercus* but afterwards it was dominated by *Pinus* alone (Roberts 1998).

178 Pollen diagrams suggest a possible change in climate from a continental to a more “Atlantic”
179 climate during the Beyşehir occupation (Bottema and Woldring 1990).

180 2.2 Chronology building

181 For further isotope analysis 15 increment cores of five living trees and seven stem discs of
182 seven dead trees were chosen from an initial sample pool comprising 54 cores and 14 stem
183 discs (Touchan et al. 2007). In general, isotopic analyses require fewer sample trees than
184 studies of tree-ring widths to provide a representative average series for a site because the
185 common signal strength among isotope series is higher (Leavitt and Long 1984; Gagen et al.
186 2004). The selection criteria for the samples were a high correlation with the mean ring-width
187 site chronology, smallest possible numbers of missing rings, no tree-ring sequences with ring
188 widths below 0.1 mm to ensure always enough sample material, no significant growth
189 suppressions and releases and no scars, reaction wood or other wound reactions to increase
190 the common signal.

191 All cores were sanded and visually cross-dated following dendrochronological procedures
192 described by Fritts (1976), Schweingruber (1983) and Cook and Kairiukstis (1990). Ring
193 widths were measured with an accuracy of 0.01 mm, using the linear table Lintab™ (Frank
194 Rinn S.A., Heidelberg, Germany) and the TSAP-Win program (Rinn 2003). The accuracy of
195 the cross-dating and measurements was verified using the computer program COFECHA
196 (Holmes 1983).

197 The samples were analysed individually and with annual resolution for $\delta^{13}\text{C}$. Tree rings were
198 split manually with a scalpel using a stereomicroscope, and the α -cellulose extracted
199 following the chemical method based on the use of sodium hydroxide and sodium chlorite
200 (Loader et al. 1997). Usually α -cellulose is extracted to concentrate on one chemical
201 compound because the different components of wood have different isotopic values (Wilson
202 and Grinsted 1977).

203 The $^{13}\text{C}/^{12}\text{C}$ isotope ratios were measured as CO_2 by combusting the α -cellulose samples in an
204 elemental analyzer (Model NA 1500; Carlo Erba, Milan, Italy) coupled via an open split to an
205 isotope ratio mass spectrometer (Micromass Optima, Ltd. Manchester, UK) operating in
206 continuous flow mode. Sample replication resulted in a precision of better than $\pm 0.1\%$ for
207 $\delta^{13}\text{C}$ values. The isotope ratios are given in the conventional delta (δ) notation, relative to the
208 standard VPDB ($\delta^{13}\text{C}$). The samples were analysed individually instead of pooling (Treydte et
209 al. 2001; Dorado Liñán et al. 2011).

210 2.3 Data analysis

211 The $\delta^{13}\text{C}$ tree-ring series are affected by the depletion in atmospheric $^{13}\text{CO}_2$ due to fossil fuel
212 burning and deforestation since the industrialization (ca. AD1850). The resulting changes in
213 the carbon isotope source value introduces a decreasing trend which is not related to tree-
214 physiological response to climatic or environmental change and needs to be removed from the
215 raw $\delta^{13}\text{C}$ tree-ring series. The most common way is to subtract annual changes in $\delta^{13}\text{C}$ of
216 atmospheric CO_2 , obtained from ice cores and direct measurements, from each tree-ring stable
217 isotope value (Leuenberger et al. 1992; Elsig et al. 2009). We applied this atmospheric
218 correction to the $\delta^{13}\text{C}$ series before any manipulation of the carbon isotope data started
219 (McCarroll and Loader 2004; Leuenberger 2007), thereby guaranteeing that the source value
220 was kept constant for the entire time period.

221 Long term changes of the atmospheric $\delta^{13}\text{C}$ source value affect all trees equally but trees may
222 respond differently to changing CO_2 concentrations. However, the persistence and extent of
223 possible plant physiological effects are still under debate. Despite experimental evidence
224 showing that elevated CO_2 levels increase growth and ^{13}C discrimination in most plants, the
225 isolation of a $\delta^{13}\text{C}$ signal consistent with anthropogenically induced rises in atmospheric CO_2
226 from the tree-ring record has shown mixed results (McCarroll et al. 2009; Beerling 1996;
227 Jahren et al. 2008). While Voelker et al. (2006) indicate that the enhancement effects of

228 elevated CO₂ on tree growth declines with age, Saurer et al. (2003) found evidence for a
229 downward adjustment of photosynthesis and diminishing isotope effects under elevated CO₂
230 only after a few years. In a recent study Schubert and Jahren (2012) comprehensively review
231 the state of the art concerning the effects of atmospheric CO₂ concentration on carbon isotope
232 fractionation. They highlight the diversity and non-linearity of the tree physiological
233 responses and therefore additional detrending methods such as the PIN correction, as recently
234 proposed by McCarroll et al. (2009), were not adopted in the current study in order not to
235 produce artificial trends.

236 After the correction of the stable carbon isotope measurements, individual series of $\delta^{13}\text{C}$ were
237 z-transformed to ensure an equal contribution of each series to the final chronology. The z-
238 transformed $\delta^{13}\text{C}$ were tested for significant autocorrelation. The $\delta^{13}\text{C}$ had a high first order
239 partial autocorrelation ($p = 0.85$, $t\text{-stat} = 26.75$) and therefore prewhitening of the series was
240 tested (Meko 1981), which however, was not found to improve the climate reconstructions.
241 Thus, prewhitening was rejected in favour of not prewhitening to preserve low-frequency
242 climatic signals in the series (Esper et al. 2003). The individual z-transformed $\delta^{13}\text{C}$ series
243 were finally averaged into one mean site chronology $\delta^{13}\text{C}_{\text{CorZ}}$ reaching back to the year
244 AD1022. The corrected and z-transformed series $\delta^{13}\text{C}_{\text{CorZ}}$ was used for further
245 dendroclimatological investigations.

246 The Expressed Population Signal (EPS, Wigley et al. 1984) was computed to assess the
247 common signal representativeness of the final chronology. Theoretically, the EPS ranges from
248 0.0 to 1.0, i.e. from no agreement to perfect agreement with the population chronology, but
249 Wigley et al. (1984) give an $\text{EPS} = 0.85$ as a reasonable limit for the chronology to still be
250 reliable.

251 2.4 Climate data

252 The most complete meteorological records closest to the study site are recorded at the
253 meteorological stations Elmali (36°44'N, 29°55'E), Isparta (37°46' N, 30°33'E) and Afyon
254 (38°45'N, 30°32'E) (Turkish General Directorate of Meteorology 2008). Monthly
255 precipitation and temperature data from the three stations were obtained to develop a regional
256 climate series representing the mountainous inland region of southwest Turkey. The three
257 stations are located at similar elevations (Elmali 1113m asl, Isparta 997m asl and Afyon
258 1034m asl). The available temperature records range from 1959 to 2000 for Elmali and from
259 1949 to 2006 at the other two stations. The time span for the precipitation data ranges between
260 1961 and 2000 in Elmali and 1931 and 2006 at the other two stations. Given the various time
261 spans of availability of the meteorological data, and in order to avoid depending on a single
262 station, we applied the method of Jones and Hulme (1996) to average the precipitation and
263 temperature records for each month since the climate data were not of the same length in
264 order to develop a mean regional series. Monthly values for each station were standardized as
265 z-scores relative to the 1959-2000 (temperature) and 1961-2000 (precipitation) common
266 periods and averaged to calculate monthly z-scores for the regional average series. These
267 monthly z-scores were converted to 'absolute' values using the average of the means and
268 standard deviations of each of the original monthly series. The complete regional temperature
269 and precipitation records extend from 1949-2006 (temperature) and 1931-2006
270 (precipitation).

271 Before relationships between climate and growth were examined we first checked the
272 meteorological data for inhomogeneities that might interfere with the tree-ring calibration
273 procedure using the techniques recommended by Mitchell et al. (1966). For the comparison
274 between stations, monthly precipitation data were summed cumulatively. The totals for one
275 station were then plotted as a function of the totals for the other station resulting in so-called
276 double mass plots. Monthly temperature data of two stations were differenced and the result

277 summed cumulatively. Only homogeneous meteorological data were then used for further
278 analysis.

279 2.5 Climate response, calibration, verification and reconstruction

280 The influence of climate on the stable isotope series was investigated by computing simple
281 linear correlations (r) with monthly climate variables using a period from January of the
282 previous year to October of the current year. The dominant climatic factor controlling tree
283 growth at Jsibeli was calibrated against the site $\delta^{13}\text{C}_{\text{CorZ}}$ tree-ring chronology. The climate
284 record was split into two periods. The first period, 2006-1978, is used for calibration and the
285 second one, 1977-1949, for the independent verification of the data. The ordinary least square
286 method was applied to find the best regression model which was then used as the transfer
287 function (Fritts 1976). The Pearson's correlation coefficient between instrumental and
288 reconstructed values, the Reduction of Error and the Coefficient of Efficiency (RE and CE;
289 Cook et al. 1994) were computed to estimate the ability of the $\delta^{13}\text{C}_{\text{CorZ}}$ data to predict the
290 selected climate factors. The verified simple linear regression model was then used to
291 reconstruct climate for the site. The 95% confidence intervals for the reconstruction were
292 calculated according to Chou (1972).

293 **3 Results and discussion**

294 The mean tree-ring width chronology, which was used for the isotope analysis, consists of 12
295 trees and covers the period from 1022 to 2006. The mixture of core samples from living trees
296 and cross sections from dead stumps and logs accounts for the smaller sample depth between
297 1980 and 2006 (Fig. 2D). The tree-ring width series display long-term trends (Fig. 2A)
298 indicating age trends which would normally be detrended if the aim was to use ring width
299 data to reconstruct climate (Touchan et al. 2003, 2007), however, in this study we
300 concentrated on stable carbon isotopes only. Between 1022 and 1124 the $\delta^{13}\text{C}_{\text{CorZ}}$ series
301 consist of less than five trees and the EPS drops below the critical value 0.85. Therefore, the

302 series was terminated in 1125 due to the small sample size in the older section and low EPS
303 values. The \bar{r}/EPS statistics for the tree-ring width and the $\delta^{13}\text{C}_{\text{CorZ}}$ chronologies are
304 0.48/0.87 and 0.44/0.85 for the period 1125 to 2006, respectively. However, it needs to be
305 mentioned that due to the small sample size of only 4 samples the EPS drops to 0.8 during the
306 period 1992 to 2006. Although, the EPS temporarily is somewhat below the critical value of
307 0.85, the overall values indicate that the mean $\delta^{13}\text{C}_{\text{CorZ}}$ chronology is a robust estimate of
308 annual changes in $\delta^{13}\text{C}$ and that it is suitable for further dendroclimatic research.

309 The raw $\delta^{13}\text{C}$ series shows a prominent decline from approximately 1900 due to the decrease
310 of atmospheric $\delta^{13}\text{C}$ values (Fig. 2B), which has been removed by the correction (Fig. 2C)
311 (Leuenberger et al. 1992; Elsig et al. 2009). The $\delta^{13}\text{C}_{\text{CorZ}}$ series exhibits relatively low values
312 in the period 1125 to the late 15th century, followed by a steady increase until the early 18th
313 century and a sharp decrease towards the late 18th century. After two peaks in the early and
314 late 19th century, the record stays relatively stable on an average level to then decrease from
315 the mid-1990s until 2006 (Fig. 2C).

316 The climate response plots present correlations between $\delta^{13}\text{C}_{\text{CorZ}}$ chronology and climate data
317 (Fig. 3). The analysis includes monthly climate data of the current (J-D) and previous (j-d)
318 year, as well as annual and selected seasonal climate data. The analysis shows significant
319 negative correlations between $\delta^{13}\text{C}_{\text{CorZ}}$ and precipitation of July to September ($r=-0.36$; $P <$
320 0.01). Highly significant correlations are shown for $\delta^{13}\text{C}_{\text{CorZ}}$ and May, January-to-March and
321 January-to-May temperatures ($r=-0.44$, $r=-0.42$ and $r=-0.52$; $P < 0.001$, respectively) (Fig. 3).

322 This leads us to the assumptions of a distinct winter-to-spring temperature signal and a weak
323 but significant summer-to-autumn precipitation signal recorded in the isotope record. The
324 negative correlations suggest that the lower the temperatures in January to May and the lower
325 the precipitation in July to September, the higher the values of $\delta^{13}\text{C}_{\text{CorZ}}$. The negative
326 correlation of the mean $\delta^{13}\text{C}_{\text{CorZ}}$ chronology with winter-to-spring temperatures indicates
327 growth stress due to low temperatures which is not surprising for a site with trees growing at

328 altitudes of 1850 to 2020 m above sea level. Basically, the discrimination of the stable carbon
329 isotopes depends on the stomatal conductance and the rate of photosynthesis (Farquhar et al.
330 1982). In winter-to-spring at such high elevations the rate of photosynthesis seems to be
331 affected mainly by low temperatures. Years with cold winter and spring temperatures are
332 likely to affect growth in two ways. In cold winters during dormancy the cambium and the
333 leaves may be damaged more than usual and the following recovery in spring may take
334 longer. Similar results have been described for pine trees in Sweden and northeast Germany
335 (Troeng and Linder 1982; von Lührte 1991). Low spring temperatures may further delay the
336 photosynthesis or slow down the rate of photosynthesis which will have negative effects on
337 the cambial activity. In contrast, the non-significant correlations between $\delta^{13}\text{C}_{\text{CorZ}}$ and winter-
338 to-spring precipitation demonstrates that stable carbon isotopes are not such a good proxy for
339 precipitation as has been demonstrated for tree-ring width (Touchan et al. 2007). It seems as if
340 the site receives enough moisture in form of snow and rainfall during the cold season.
341 However, other proxies such as stable oxygen isotopes may be able to reveal a stronger
342 moisture signal. During the summer-to-autumn period, humidity levels in the soil and the air
343 turn low, and hence fractionation is depending more on the stomatal conductance which
344 seems to change throughout the season due to the increasing vapor pressure deficit. Since
345 $\delta^{13}\text{C}_{\text{CorZ}}$ correlated best with the temperature data, the mean January-to-May temperatures
346 were calibrated against $\delta^{13}\text{C}_{\text{CorZ}}$ in tree rings.

347 The regression analysis between $\delta^{13}\text{C}_{\text{CorZ}}$ and the January-to-May temperature for the entire
348 period 1949 to 2006 determined the linear relationship $y = -1.1735x + 7.3414$. The correlation
349 $r = 0.42$ ($P < 0.001$) is highly significant for the calibration period (1978-2006) and also for
350 the verification period 1949 to 1977 ($r = 0.61$; $P < 0.001$), and 27% of the $\delta^{13}\text{C}_{\text{CorZ}}$ variation is
351 explained by the January-to-May temperature data. The reduction of error (RE) and
352 coefficient of efficiency (CE) were calculated (Tab. 1) to provide an indication of the
353 robustness of the relationship between $\delta^{13}\text{C}_{\text{CorZ}}$ and the January-to-May temperature.

354 Although the values are not very high ($RE = 0.29 / CE = 0.28$) both values are positive. The
355 theoretical limits for the RE and CE statistics range from 1 which indicates perfect agreement
356 to minus infinity. A minus value indicates no agreement but any positive value can be
357 considered as encouraging (Fritts 1976).

358 Observed and modelled temperature values show only a few differences during the calibration
359 and verification periods. In the calibration period more differences are apparent but generally
360 the model follows the course of the observed data (Fig. 4). Nevertheless, the statistics indicate
361 that the reconstruction is of good quality and stable in time. Based on the established climate
362 growth relationship we here present the reconstruction of January-to-May temperature (Fig.
363 5).

364 The temperature reconstruction exhibits multi-decadal to centennial variability with winter-to-
365 spring temperatures mostly above average for the period 1125 and 1510. The medieval warm
366 period (MWP) is reflected by temperatures being constantly above the average between the
367 early 12th and mid-14th century. Then temperatures decrease until 1700 with only a short
368 increase around 1625. The little ice age (LIA) heralds itself by low values in the temperature
369 reconstruction with the beginning of a decreasing temperature trend in 1475, and the LIA
370 finally is in full swing during the 17th and 18th centuries, as indicated by very low reconstructed
371 temperatures. The first winter-to-spring temperature minimum in 1700 is followed by a short
372 increase until approximately 1730 to then drop again to the second absolute low in 1750.
373 These two minima together with a third in the mid-19th century are generally agreed on and
374 have been found elsewhere (Grove 1988).

375 When compared to well-known activity events of the Sun (Solanki et al. 2004) our
376 reconstruction confirms high temperatures for periods of high solar activity during the
377 Medieval Warm Period and low temperatures during large parts of the Wolf (1300-1380),
378 Spörer (1480-1550), Maunder (1645-1715) and Dalton Minima (1790-1820). The modern

379 solar maximum since the 1950s is reflected by higher reconstructed temperatures but only
380 since the 1990s.

381 **3.1 Comparison with documentary data**

382 Comparing climate reconstructions based on proxies with historical documentary data often
383 confirms that extremely narrow or wide rings were caused by severe climate conditions which
384 not only had a significant impact on tree growth but at the same time had detrimental effects
385 on the societies affected. Documentary data usually record extreme events such as very cold
386 or prolonged drought periods (Hammer-Purgstall 1834-1836; Panzac 1985; Brázdil et al.
387 2005; Telelis 2005, 2008). Since documentary records from the Eastern Mediterranean mainly
388 report extreme drought or flooding events (Kuniholm 1990), only a small number of written
389 records regarding extreme temperature deviations can be found in the literature. Telelis (2005,
390 2008) analysed historical information from the time of the Byzantine Empire and grouped his
391 results into cold, hot, wet and dry episodes. In the mediterranean to temperate semi-arid
392 climate regions (Csa and BSk, respectively), Telelis (2005, 2008) identified the years 1230-
393 1300, 1320-1400 and 1430-1450 as periods with a higher frequency of cold episodes, that is,
394 with more than two cold events of long duration per decade. All three cold periods are also
395 indicated by our reconstruction, however, extremely hot years were not identified neither by
396 our data nor by the historical records. Kuniholm (1990) reviewed several historical records
397 and found mainly hints to dry and hot summers. The only mention of cold temperatures is for
398 the winter of 1611 to 1612 which must have been exceptionally rich in snow because notes
399 were made for awful snow in Anatolia and that the French consul in Turkey was killed when
400 heavy snow broke through his house. In our record the winter of 1611 to 1612 is only
401 indicated as slightly below average, however, heavy snow does not necessarily mean low
402 temperatures. The German traveller Naumann (1893) reported that the years 1873 and 1874
403 had devastating effects on the Turkish society. A very dry and hot summer 1873 followed by

404 very cold winter 1873 to 1874 killed 150000 people and 100000 head of livestock. In our
405 record the January-to-May temperature of 1874 is also one of the lowest since 1125 thereby
406 corroborating the historical records.

407 **3.2 Temperature trends**

408 Remarkably, our winter-to-spring temperature reconstruction does not follow the 20th century
409 warming trend, found elsewhere (Wahl et al. 2010). In fact, for most of the 20th century we
410 have reconstructed relatively low winter-to-spring temperatures and our reconstruction
411 suggests that temperatures are only increasing since the 1980s.

412 The temperature trends in our reconstruction are in line with trend analysis results of
413 meteorological data from Turkey and other parts of the eastern Mediterranean. Based on the
414 analyses of 85 individual station data in Turkey (Türkeş et al. 1995; Kadioglu 1997), general
415 decreasing trends in annual and seasonal mean surface air temperature series over much of
416 Turkey were found. In particular, the coastal regions of Turkey were largely characterized by
417 colder than long-term average temperature conditions during the period between the late
418 1960s and early 1990s. Nevertheless, this trend has begun to change recently in Turkey,
419 particularly due to increases in the mean temperature of the spring and summer seasons
420 (Türkeş et al. 2002). In the eastern Mediterranean, several studies dealing with long-term
421 variations and trends of surface air temperatures have been conducted. In Greece, Proedrou et
422 al. (1997) detected an overall cooling trend for the majority of Greek stations in winter for the
423 entire period of 1951-93. Ben-Gai et al. (1999) analysed the maximum and minimum
424 temperatures of 40 stations in Israel for the period 1964-94. They revealed that both
425 temperatures were characterized by a significant decreasing trend during the cool season and
426 by an increasing trend during the warm season. Feidas et al. (2004) found a cooling trend in
427 winter temperatures in Greece for the period 1955-2001, whereas, summer showed an overall
428 warming trend, however, neither was statistically significant. As a result, the overall trend of

429 the annual values was nearly zero. Similar conclusions can be drawn from a global analysis
430 by Schönwiese (2008) which indicates a weak decreasing trend of annual mean temperatures
431 for Turkey in contrast to the overall increasing trend for large parts of Eurasia during the last
432 100 years. Xoplaki (2002) and Luterbacher et al. (2004) also found stable or temporarily
433 decreasing temperatures for the Mediterranean in general and Turkey in particular.

434 Since previous analyses of meteorological data especially from the eastern Mediterranean
435 have indicated diverging trends regarding winter and summer temperatures, the
436 meteorological temperature data used during our reconstruction procedure were tested for
437 possible trends. The test was the basic linear regression-based model in which time t (in
438 years) was taken as the independent variable and temperature as the dependent variable.

439 Under the usual regression assumptions a two-tailed t-test was conducted where the null
440 hypothesis states that the slope coefficient is equal to 0. If this is true, then there is no linear
441 relationship between the explanatory and dependent variables, i.e., no trend can be identified
442 (Bahrenberg et al. 1990). Similar to the findings by Türkeş et al. (2002), the climate data used
443 for the current study also revealed long-term trends between 1950 and 2006 (Fig. 6).

444 While in spring and autumn no obvious trends are visible, positive and negative trends in
445 summer and winter, respectively, are noticeable. The slope parameter estimates are all
446 positive, except for winter, however, the t-test statistics are only significant for summer. The
447 trend analysis of meteorological data has identified similar seasonal trends as in Greece and
448 Israel where increasing summer temperatures and decreasing winter temperatures have also
449 been found (Proedrou et al. 1997; Ben-Gai et al. 1999; Feidas et al. 2004).

450 Since the existing studies and the trend analysis of the climate data suggest that dissimilar
451 seasonal temperature trends are present at several locations not only in Turkey but in other
452 Mediterranean countries as well, the 20th century temperature rise missing in our
453 reconstruction cannot be regarded as an analysis artefact but seems to be a rather special
454 feature of the climate in parts of Turkey and surrounding countries of the Mediterranean.

455 **3.3 Comparison with other temperature reconstructions**

456 The review of existing literature brought to light that no local temperature reconstructions
457 based on tree rings are available from the Eastern Mediterranean. Due to this lack of material
458 for direct comparison, our Turkish temperature reconstruction was compared to a collection of
459 92 regional, hemispherical and global temperature reconstructions (Wahl et al. 2010). Wahl et
460 al. (2010) describe a newly integrated archive of high-resolution temperature reconstructions
461 for the last 2000 years included in NOAA's National Climatic Data Center, from small
462 regional to global scale. The 92 surface temperature records including global, hemispheric,
463 regional, and local single time series reconstructions were downloaded from the PaleoClimate
464 Network (PCN v. 2.0.0) at <http://www.ncdc.noaa.gov/paleo/pubs/pcn/pcn.html>. Most of the
465 records reconstruct annual mean temperatures with annual resolution for the last Millennium
466 (Wahl et al. 2010). The reconstructions were compared with our Turkish reconstruction by
467 means of simple Pearson's correlation analysis and those correlating best with it were selected
468 for further examination.

469 The correlation analysis revealed that many of the records do not correlate well with our
470 Turkish reconstruction. Several reasons may be held responsible: many of the records are less
471 suitable because they are local or regional reconstructions far away from Turkey, they are
472 reconstructions for other seasons and the reconstructions are shorter or have a lower
473 resolution.

474 From the 92 reconstructions those of Moberg et al. (2005) and Mann et al. (2008) were
475 selected for further examination because they correlated best over the entire common period
476 of 881 years. The correlation was more specified by comparing high-, band-, and low-pass
477 filtered versions of the series (Fig. 7). The filtering was achieved by calculating the 11- and
478 61-year centred moving averages of the individual series which was followed by a
479 decomposition of the original data into the three different components. The correlation
480 patterns, separated into the three different frequency domains, revealed that the two

481 hemispherical temperature reconstructions agree with our Turkish reconstruction only in the
482 low frequency indicated by highly significant correlations.

483 When plotted together it is obvious that the three temperature reconstructions share common
484 long-term trends (Fig. 8). All three records show above average temperatures during the
485 medieval period and also some similar decadal-scale variations. They also contain a long-term
486 descent to an all-time low at around 1700 and then temperatures start to increase again,
487 however, the Turkish reconstruction does not follow the temperature rise indicated by the two
488 hemispherical reconstructions during the 20th century.

489 In other frequency domains no strong correlations were identified which may be explained by
490 the fact that most of the records used for the two hemispherical temperature reconstructions
491 were derived from proxies located much further to the north. Temperature proxies from the
492 north such as the European Alps, Scandinavia or Russia may be too far away from our
493 Turkish reconstruction to contain the same high-frequency signals because the limiting factors
494 of tree growth are too site-specific and differ too much inter-annually. Furthermore, the
495 hemispherical records are annual mean temperatures while our Turkish reconstruction is a
496 January-to-May temperature proxy.

497 **3.4 Spatial correlation and spectral analysis**

498 While the correlations with other temperature proxies were high only in the low-frequency
499 domain, in a next step it was also interesting to spatially correlate our $\delta^{13}\text{C}_{\text{CorZ}}$ record with
500 gridded winter-to-spring temperature data, in order to identify the geographic regions with
501 significant correlations between temperature and our $\delta^{13}\text{C}_{\text{CorZ}}$ record. We used the KNMI
502 Climate Explorer website (<http://www.knmi.nl/>) (van Oldenborgh and Burgers 2005) to
503 generate correlation fields with seasonal January-to-May temperatures.

504 The spatial field correlations indicate that our $\delta^{13}\text{C}_{\text{CorZ}}$ record does not correlate with any
505 January-to-May temperature grids in Northern or Central Europe during the analysis period

506 2006 to 1949 (Fig. 9). However, the map demonstrates that, intriguingly, most of the field
507 correlation is oriented towards the south and east of the study site, that is, the spatial
508 correlation between the $\delta^{13}\text{C}_{\text{CorZ}}$ chronology and the January-to-May mean temperature covers
509 an area of most of Turkey, Syria and northeast Africa.

510 From this spatial analysis the question may arise what is actually influencing temperature
511 variations in Turkey. The graphical oscillation patterns of the reconstructed January-to-May
512 mean temperature and its 61-year moving average (Fig. 5 and 8) already suggests the presence
513 of some low-frequency variability.

514 For further analysis of such possible non-random variations our temperature reconstruction
515 was subjected to a spectral analysis to decompose it into different frequencies and analyse the
516 variance in each frequency band to uncover possible trends and periodicities (Jenkins and
517 Watts 1968). The software package Autosignal (Systat) determines those spectral density
518 values that appear particularly strong and enables an easy graphical estimation of possible
519 trends within the chronology (Davis 1986). The spectral analysis plot investigates possible
520 reoccurring cycles (Fig. 10). Significant peaks at approximately 26, 32, 40, 55 and 87 years
521 can be identified. Such multi-decadal peaks fall into the bandwidths of various climate indices
522 such as the North Atlantic Oscillation (NAO), Arctic Oscillation (AO) or Mediterranean
523 Oscillation (MO). Since some of the spectral peaks are similar to those known from
524 prominent climate indices, we decided to compare our temperature reconstruction with a
525 selection of such climate indices to identify likely candidates for having an influence on the
526 reconstructed winter-to-spring temperatures in SW-Turkey.

527 **3.5 Comparison of temperature reconstruction with circulation indices**

528 The North Atlantic Oscillation (NAO) is the most important large scale mode of climate
529 variability in the Northern Hemisphere. The NAO describes a large scale meridional
530 fluctuation of atmospheric masses between the North Atlantic regions of the subtropical

531 anticyclone near the Azores and the subpolar low pressure system near Iceland. The North
532 Atlantic Oscillation (NAO) has been shown to be connected to the interannual variability of
533 climatic conditions in the Mediterranean (Hurrell 1996; Werner and Schönwiese 2002).

534 The Arctic Oscillation (AO) is a teleconnection pattern characterized by a seesaw of
535 atmospheric pressure between the Arctic and northern middle latitudes (Thompson and
536 Wallace 1998). When the AO index (AOI) is positive, changes in the circulation patterns
537 bring cooler and drier conditions to the Mediterranean basin. The negative phase is
538 characterized by warmer and wetter conditions in the Mediterranean. Some studies have
539 shown that the AO is closely connected to the interannual variability of mid- to high-latitude
540 climates (e.g., Wang et al. 2005).

541 Conte et al. (1989) suggested the existence of the so-called Mediterranean Oscillation (MO)
542 which reflects a dipole or seesaw effect between Alger and Cairo mean annual geopotential
543 heights at the 500 hPa level. Based on this concept, a dipole-behaviour of the temperatures
544 between the western and eastern Mediterranean have been attributed to the MO (Kutiel and
545 Maheras 1998; Maheras and Kutiel 1999). Favourable conditions for high temperatures in one
546 part are associated with unfavourable conditions in the other part and *vice versa*.

547 Kutiel and Benaroch (2002) identified a new seesaw feature they named the North Sea-
548 Caspian Pattern (NCP). They defined the NCP as an upper level atmospheric teleconnection
549 between the North Sea and the northern Caspian. The North Sea-Caspian Pattern Index
550 (NCPI) is negative most of the year. Negative NCPI episodes are more frequent than positive,
551 but during the 1990s there has been an increase in positive NCPI episodes.

552 The East Atlantic/West Russia (EAWR) pattern is a prominent teleconnection pattern that
553 affects Eurasia throughout the year (Barnston and Livezey 1987). During the negative
554 (positive) EAWR phases, wetter (drier) than normal weather conditions are observed over a
555 large part of the Mediterranean (Krichak and Alpert 2005).

556 The El Niño Southern Oscillation (ENSO) is a climate pattern that occurs across the tropical
557 Pacific Ocean. The term El Niño (La Niña) refers to warming (cooling) of the central and
558 eastern tropical Pacific Ocean which leads to a major shift in weather patterns every three to
559 eight years across the Pacific. ENSO is the oscillation between El Niño and La Niña
560 conditions (Allan et al. 1996).

561 The Indian Ocean Dipole Mode Index (DMI), as defined by Saji et al. (1999), is an indicator
562 of the east-west sea surface temperature (SST) gradient across the tropical Indian Ocean,
563 linked to the Indian Ocean dipole mode, a zonal mode of the interannual variability of the
564 Indian Ocean. A positive (negative) DMI is defined as above (below) normal SST in the
565 tropical western Indian Ocean and below (above) normal SST in the tropical eastern Indian
566 Ocean (Saji et al. 1999). Associated with a positive DMI phase are surplus Indian summer
567 monsoon rainfall and an intensified upward motion of air over India. The associated divergent
568 flow in the upper troposphere progresses westward and converges over the Mediterranean
569 where the descent of air is intensified, constructing a zonal-vertical circulation cell from the
570 northern India towards the Mediterranean region (Guan and Yamagata 2003).

571 Since all the above climate indices have the potential to influence the temperature variation in
572 Turkey, monthly and seasonally averaged indices of the indices were correlated with our
573 Turkish January-to-May temperature reconstruction (Tab. 2). Since the indices MOI, NCPI
574 and EAWR reach back only to the 1950s, all correlations were computed for the period 1950
575 to 2006 maximising their comparability with the other indices.

576 The correlations for NAO and AO are negative for May-to-June of the previous year and
577 March-to-May of the current year, and the strongest correlation is indicated between the
578 January-to-May temperature reconstruction and the AOI of May-to-June of the previous year.
579 Xoplaki (2002) also showed negative correlations between NAO and temperatures in winter
580 for the Eastern Mediterranean. Statistically significant negative relationships between winter
581 temperatures and the winter NAO Index were discovered in Israel (Ben-Gai et al. 2001), in

582 Egypt (Hasanean 2004), Greece (Feidas et al. 2004) and Turkey (Türkeş and Erlat 2009).
583 Wang et al. (2005) revealed that negative AO phases correspond to warm conditions in
584 Turkey and the Middle East. Xoplaki (2002) showed that the influence of the negative winter
585 AO on the Mediterranean climate was generally towards warmer and drier conditions over the
586 southern and eastern parts of the Mediterranean region including Turkey. Türkeş and Erlat
587 (2008) revealed significant negative correlations between the variability of winter mean
588 temperatures in Turkey and the AO.

589 The correlation between our temperature reconstruction and the MOI was negative but low for
590 most of the months. We only identified a significant negative correlation in August of the
591 previous year. In comparison, in the eastern Mediterranean a negative correlation between the
592 MOI and winter temperature has been found (Feidas et al. 2004), i.e., when the MOI was in a
593 positive (negative) phase, temperatures in the eastern Mediterranean were below (above)
594 average. The relationship between NCPI and the January-to-May temperature reconstruction
595 is characterized by positive correlations in July and October of the previous year and negative
596 correlations in April to May of the previous year and February to April of the current year.
597 Kutiel and Türkeş (2005) also found negative correlations which meant that negative NCPI
598 episodes tended to cause above normal temperatures in Turkey. In a comprehensive
599 comparison, Türkeş and Erlat (2009) demonstrated that the NCPI and the AO are more
600 capable than the NAO for explaining the year-to-year temperature variability in Turkey. The
601 correlation between the EAWR index and the January-to-May temperature reconstruction is
602 positive in June and negative in August, both months of the previous year. Over the eastern
603 Mediterranean region positive (negative) EAWR winter periods are associated with more
604 (less) intense northern air flows (Krichak et al. 2002), which result in below (above) average
605 temperature conditions in the eastern Mediterranean.

606 Significant positive correlations resulted from the comparison between the January-to-May
607 temperature reconstruction and NINO4 and DMI. Positive correlations are illustrated for May,

608 June and August of the previous year. Similarly, in the Eastern Mediterranean there is some
609 evidence that El Niño events are positively correlated with winter rainfall (Kadioglu et al.
610 1999). On the other hand, Pozo-Vázquez et al. (2005) found a non-linear response to ENSO in
611 the Eastern Mediterranean. Negative precipitation anomalies with similar amplitude
612 anomalies occurred both during El Niño and La Niña events. During El Niño events
613 meridional shifts of the jet stream have been observed in the Eastern Mediterranean (Alpert et
614 al. 2006). Other relationships between Eastern Mediterranean weather conditions and ENSO
615 have been suggested, but these are generally weak or not stable (Xoplaki 2002). The strongest
616 descent of the Indian Ocean dipole mode (DMI) circulation pattern, which has also been
617 coined monsoon-desert mechanism (Rodwell and Hoskins 1996), is centered over the eastern
618 Mediterranean, covering southeastern Europe and the eastern Sahara desert, where it is likely
619 to inhibit convection and to cause dry or arid conditions (Saji and Yamagata 2003).

620 The climate indices NINO4 and DMI are mainly associated with climatic influences coming
621 from the southeast and they are positively correlated with the January-to-May temperature
622 reconstruction. In comparison, positive phases of the two indices seem to result in higher
623 January-to-May temperatures while positive phases of all the other indices seem to cause
624 below-average temperatures in winter to spring.

625 Furthermore, the analysis illustrates that our temperature reconstruction is more correlated to
626 the climate index values of the previous year than of the current, although for two indices, that
627 is, AO and NCPI, significant correlations are also shown for February-to-May of the current
628 year. This suggests an often delayed reaction of the trees to changes of the climate indices.
629 However, the climate indices themselves do not alter tree growth directly but the indices
630 indicate changing climate conditions responsible for tree growth alterations. It seems likely
631 that changing indices in the middle of the previous year indicate climate shifts which impact
632 on tree growth, delayed by several months, in the next year.

633 The fact that various climate indices seem to have significant effects on the reconstructed
634 temperature variations suggests that the climate at the study site in Southwest Turkey is
635 affected by a mixture of climate mechanisms which are responsible for the temperature
636 variations limiting Juniper tree growth in SW Turkey. At least two reasons can be proposed
637 that may explain the mixture of correlations with all indices. The first is that some of the
638 indices also correlate with each other since they describe similar or related oscillation
639 patterns, such as the NAO, AO and NCPI. The second reason is that the correlation between
640 the temperature and the indices is unstable in time which would indicate that in some years
641 the temperature variations in Southwest Turkey are more influenced by one index while in the
642 following years they are more affected by others as has been identified similarly in Australia
643 (Heinrich et al. 2009).

644 For a more detailed analysis of this second scenario of different influences, correlations
645 between the January-to-May temperature reconstruction and January-to-May averages of the
646 climate indices were calculated in moving windows of 13 years (Heinrich et al. 2009). We
647 found varying correlations in time between the reconstruction and indices (due to different
648 lengths of the indices separated into Figs. 11 and 12). This result explains the limited
649 correlations between our reconstruction and the indices when analysing them for the entire
650 period. The correlations of the shorter series with our temperature reconstruction suggest
651 significant values for the EAWR only between 1975 and 1990 (Fig. 11). The correlations
652 between our reconstruction and the MOI and the EAWR, respectively, run mostly in opposite
653 direction which indicates that temperature variations in some years are more influenced by
654 Mediterranean atmospheric oscillation patterns and in other years by the East Atlantic West
655 Russia pattern.

656 The correlations of the longer series with our temperature reconstruction also give some
657 insights into the temporal dynamics of the relationships. The similar correlations between our
658 reconstruction, NAO and AO, respectively, suggest that both climate indices represent related

659 atmospheric oscillation patterns which have comparable influences on the temperature
660 variations in Southwest Turkey. The correlation between our temperature reconstruction and
661 NAO and AO runs in opposite direction to the correlation between the reconstruction and the
662 DMI (Fig. 12). The same holds true for the correlations of the reconstruction with the DMI
663 and NINO4, respectively. While in some years the climate in Turkey seems to be influenced
664 by varying atmospheric conditions coming from the West to Northwest indicated by good
665 correlations with NAO and AO, in other years it is influenced more by Southeastern
666 atmospheric oscillation patterns suggested by good correlations with DMI and NINO4. The
667 results substantiate expectations for the climate in Turkey situated in a transitional zone
668 between the temperate zone of central and northern Europe affected by westerly flows, the
669 arid zone of the subtropical high of North Africa and in the periphery of the monsoonal
670 system acting in the Southeast. Overall, such correlation patterns changing synchronously
671 imply that the climate in Southwest Turkey is influenced by various atmospheric oscillation
672 patterns as has previously been indicated for the Eastern Mediterranean by Feidas et al.
673 (2004), Xoplaki (2002) and Luterbacher et al. (2004).

674 **4 Conclusions**

675 We have presented the first precisely dated and climatically sensitive stable carbon isotope
676 tree-ring chronology for Turkey where heretofore there were no such tree-ring proxies
677 available. The $\delta^{13}\text{C}_{\text{CorZ}}$ mean chronology showed significant negative correlations with
678 summer precipitation and January-to-May temperatures, which lead us to the assumptions of a
679 distinct winter-to-spring temperature signal and a weak but significant summer-to-autumn
680 precipitation signal recorded in the isotope record. Since results of previous studies from the
681 eastern Mediterranean indicated temporally changing temperature trends which also differed
682 seasonally and between the countries, our new reconstruction is interesting in particular
683 regarding its long-term behaviour. In the absence of any other high resolution temperature

684 proxy from Turkey our new temperature reconstruction is a valuable addition to the regional
685 proxy data in the eastern Mediterranean. Low-frequency variations, which were associated
686 with the medieval warm period and the little ice age, were identified in the winter-to-spring
687 temperature reconstruction, however, the 20th century warming trend found elsewhere could
688 not be identified in our temperature proxy record. The analysis of the corresponding
689 meteorological data used for our study and results of temperature trend analyses conducted
690 previously by others in the Eastern Mediterranean corroborated our result that the winter-to-
691 spring temperatures in the region have not increased during the 20th century. Comparisons
692 with other proxy data from the Northern Hemisphere showed that similar low-frequency
693 signals can be identified until the beginning of the 20th century when other proxies derived
694 from further north indicate a significant warming. The spatial correlation patterns
695 demonstrated strong links between our $\delta^{13}\text{C}_{\text{CorZ}}$ chronology and the January-to-May mean
696 temperatures from the Eastern Mediterranean and northeast Africa but no links to northern
697 and central Europe. The temperature reconstruction revealed multi-decadal oscillations
698 ranging between 87 and 26 years which are in the frequency range of some prominent
699 atmospheric oscillation patterns such as NAO. The variety of oscillations contained by the
700 $\delta^{13}\text{C}_{\text{CorZ}}$ chronology suggests that the atmospheric oscillation patterns are capable of
701 influencing the temperature variations in Southwest Turkey. Correlation analyses including
702 our temperature reconstruction and seven well-known climate indices which represent
703 atmospheric oscillation patterns possibly impacting the study region illustrated temporally and
704 geographically changing links between our reconstruction and the oscillation patterns. In
705 some instances the correlations ran in opposite directions which implied complex
706 relationships between the climate patterns. A multi-proxy approach comprising chronologies
707 of tree-ring width, stable isotopes, wood density and quantitative wood anatomy
708 measurements seems indispensable to better understand the long-term climate dynamics in the

709 Eastern Mediterranean, particularly in Turkey where so far only tree-ring width series have
710 been used as high-resolution proxies.

711 **Acknowledgements**

712 We thank Carmen Bürger and Christoph Küppers for their help in the laboratory. This
713 research was funded by the EU project MILLENNIUM (#017008).

714

715 **References**

716 Akkemik Ü (2000) Dendroclimatology of umbrella pine (*Pinus pinea* L.) in Istanbul (Turkey). Tree-ring

717 Bull 56:17–20

718 Akkemik Ü (2003) Tree rings of *Cedrus libani* at the northern boundary of its natural distribution.

719 IAWA J 24:63–73

720 Akkemik Ü, Aras A (2005) Reconstruction (1689–1994) of April-August precipitation in southwestern

721 part of central Turkey. Int J Climatol 25:537–548

722 Akkemik Ü, Dagdeviren N, Aras A (2005) A preliminary reconstruction (A.D. 1635–2000) of spring

723 precipitation using oak tree rings in the western Black Sea region of Turkey. Int J Biomet 49:297–

724 302. doi:10.1007/s00484-004-0249-8

725 Akkemik Ü, D'Arrigo R, Cherubini P, Köse N, Jacoby GC (2008) Tree-ring reconstructions of

726 precipitation and streamflow for north-western Turkey. Int J Climatol 28:173–183

727 Allan R, Lindesay J, Parker D (1996) El Niño southern oscillation and climatic variability. CSIRO

728 Publishing, Collingwood, Australia

729 Alpert P, Baldi M, Ilani R, Krichak S, Price C, Rodó X, Saaroni H, Ziv B, Kishcha P, Barkan J, Mariotti A,

730 Xoplaki E (2006) Relations between climate variability in the Mediterranean region and the

731 tropics: ENSO, South Asian and African monsoons, hurricanes and Saharan dust. In: Lionello P,

732 Malanotte-Rizzoli P, Boscolo R (eds) Mediterranean Climate Variability. Elsevier, Amsterdam, pp

733 149–177

- 734 Bahrenberg G, Giese E, Nipper J (1990) *Statistische Methoden in der Geographie*. Bd. 1 Univariate
735 und bivariate Statistik. Teubner, Stuttgart
- 736 Barnston A G, Livezey RE (1987) Classification, seasonality and persistence of low-frequency
737 atmospheric circulation patterns. *Mon Wea Rev* 115:1083–1126
- 738 Ben-Gai T, Bitan A, Manes A, Alpert P, Rubin S (1999) Temporal and spatial trends of temperature
739 patterns in Israel. *Theor Appl Climatol* 64:163–177
- 740 Ben-Gai T, Bitan A, Manes A, Alpert P, Kushnir Y (2001) Temperature and surface pressure anomalies
741 in Israel and the North Atlantic Oscillation. *Theor Appl Climatol* 69:171–177
- 742 Beerling D J (1996) ^{13}C discrimination by fossil leaves during the late-glacial climate oscillation 12–10
743 ka BP: measurements and physiological controls. *Oecologia* 108:29–37
- 744 Bottema S, Woldring H (1990) Anthropogenic indicators in the pollen record of the Eastern
745 Mediterranean. In: Bottema S, Entjes-Nieborg G, van Zeist W (eds) *Man's role in the shaping of*
746 *the eastern Mediterranean landscape*. Balkema, Rotterdam, pp 231–64
- 747 Brázdil R, Pfister C, Wanner H, von Storch H, Luterbacher J (2005) Historical climatology in Europe -
748 the state of the art. *Clim Change* 70:363–430
- 749 Chou Y (1972) *Probability and statistics for decision making*. Holt, Rinehart, Winston, NY
- 750 Conte M, Giuffrida S, Tedesco S (1989) The Mediterranean oscillation: impact on precipitation and
751 hydrology in Italy. In: *Proceedings of the Conference on Climate and Water 1*. Publications of
752 Academy of Finland, Helsinki, pp 121–137
- 753 Cook ER, Kairiukstis LA (1990) *Methods of Dendrochronology*. Kluwer, Dordrecht, Netherlands
- 754 Cook ER, Briffa KR, Jones PD (1994) Spatial regression methods in dendroclimatology: A review and
755 comparison of two techniques. *Int J Climatol* 14:379–402
- 756 Corte-Real J, Zhang X, Wang X (1995) Large-scale circulation regimes and surface climatic anomalies
757 over the Mediterranean. *Int J Climatol* 15:1135–1150
- 758 D'Arrigo R, Cullen HM (2001) A 350-year (AD 1628–1980) reconstruction of Turkish precipitation.
759 *Dendrochronologia* 19:169–177
- 760 Davis JC (1986) *Statistics and data analysis in Geology*. 2nd Edition. John Wiley & Sons, New York

- 761 Dorado Liñán I, Gutierrez E, Helle G, Heinrich I, Andreu-Hayles L, Plannels O, Leuenberger M, Bürger
762 C, Schleser G (2011) Pooled versus separate measurements of tree-ring stable isotopes. *Sci Total*
763 *Environ* 409:2244–2251
- 764 Elsig J, Schmitt J, Leuenberger D, Schneider R, Eyer M, Leuenberger M, Joos F, Fischer H, Stocker TF
765 (2009) Stable isotope constraints on Holocene carbon cycle changes from an Antarctic ice core.
766 *Nature* 461:507–510. doi:10.1038/nature08393
- 767 Esper J, Cook ER, Krusic PJ, Peters K, Schweingruber FH (2003) Tests of the RCS method for preserving
768 low-frequency variability in long tree-ring chronologies. *Tree-Ring Res* 59:81–98
- 769 Farquhar GD, O’Leary MH, Berry JA (1982) On the relationship between carbon isotope
770 discrimination and the intercellular carbon dioxide concentration in leaves. *Aust J Plant Physiol*
771 9:121–137
- 772 Feidas H, Makrogiannis T, Bora-Senta F (2004) Trend analysis of air temperature time series in Greece
773 and their relationship with circulation using surface and satellite data: 1955–2001. *Theor Appl*
774 *Climatol* 79:185–208
- 775 Fritts HC (1976) *Tree Rings and Climate*. Blackburn Press, Caldwell, NJ
- 776 Gagen M, McCarroll D, Edouard J-L (2004) Latewood width, maximum density, and stable carbon
777 isotope ratios of pine as climate indicators in a dry subalpine environment, French Alps. *Arct*
778 *Antarct Alp Res* 36:166–171
- 779 Gagen M, McCarroll D, Edouard J-L (2006) Combining tree ring width, density and stable carbon
780 isotope series to enhance the climate signal in tree rings: an example from the French Alps. *Clim*
781 *Change* 78:363–379
- 782 Gassner G, Christiansen-Weniger F (1942) Dendroklimatologische Untersuchungen über die
783 Jahresringentwicklung der Kiefern in Anatolien. *Nova Acta Leopold* 12:1-137
- 784 Griggs CB, Degaetano AT, Kuniholm PI, Newton MW (2007) A regional reconstruction of May-June
785 precipitation in the north Aegean from oak tree-rings, AD 1089-1989. *Int J Climatol* 27, 1075–1089
- 786 Grove JM (1988) *The Little Ice Age*. Methuen, London

- 787 Guan Z, Yamagata T (2003) The unusual summer of 1994 in East Asia: IOD Teleconnections. *Geophys*
788 *Res Lett.* doi:10.1029/2002GL016831
- 789 von Hammer-Purgstall J (1834-1836) *Geschichte des osmanischen Reiches*. Pesth, Hartleben
- 790 Hasanean HM (2004) Wintertime surface temperature in Egypt in relation to the associated
791 atmospheric circulation. *Int J Climatol* 24:985–999. doi:10.1002/joc.1043
- 792 Heinrich I, Weidner K, Helle G, Vos H, Lindesay J, Banks JCG (2009) Interdecadal modulation of the
793 relationship between ENSO, IPO and precipitation: insights from tree rings in Australia. *Climate*
794 *Dyn* 33: 63–73. doi:10.1007/s00382-009-0544-5
- 795 Holmes RL (1994) *Dendrochronology Program Manual*. Laboratory of Tree-ring Research. Tucson,
796 Arizona
- 797 Hughes MK, Kuniholm PI, Garfin GM, Latini C, Eischeid J (2001) Aegean tree-ring signature years
798 explained. *Tree-ring Research* 57:67–73
- 799 Hughes MK, Swetnam TW, Diaz HF (2010) *Dendroclimatology: Developments in Paleoenvironmental*
800 *Research*
- 801 Hurrell JW (1996) Influence of variations in extratropical wintertime teleconnections on Northern
802 Hemisphere temperature. *Geophys Res Lett* 23:665–668
- 803 Jahren AH, Arens NC, Harbeson SA (2008) Prediction of atmospheric $\delta^{13}\text{CO}_2$ using fossil plant tissues.
804 *Rev Geophys* 46:1–12
- 805 Jenkins GM, Watts DG (1968) *Spectral analysis and its applications*. Holden-Day, San Francisco
- 806 Jones PD, Hulme M (1996) Calculating regional climatic time series for temperature and
807 precipitation: methods and illustrations. *Int J Climatol* 16:361–377
- 808 Kadioğlu M (1997) Trends in surface air temperature data over Turkey. *Int J Climatol* 17:511–520
- 809 Kadioğlu M, Tulunay Y, Borhan Y (1999) Variability of Turkish precipitation compared to El Nino
810 events. *Geophys Res Lett* 26:1597–1600
- 811 Köse N, Akkemik Ü, Dalfes HN, Özeren MS (2011): Tree-ring reconstructions of May-June
812 precipitation for western Anatolia. *Quat Res* 75:438–450. doi:10.1016/j.yqres.2010.12.005

- 813 Krichak SO, Kishcha P, Alpert P (2002) Decadal trends of main Eurasian oscillations and the
814 Mediterranean precipitation. *Theor Appl Climatol* 72:209–220
- 815 Krichak SO, Alpert P (2005) Decadal trends in the east Atlantic–west Russia pattern and
816 Mediterranean precipitation. *Int J Climatol* 25:183–192. doi:10.1002/joc.1124
- 817 Kuniholm PE (1990) Archaeological evidence and non-evidence for climatic change. In: Runcorn SJ,
818 Peckers J-C (eds) *The Earth's climate and variability of the sun over recent millennia*. Philosophical
819 Transactions of the Royal Society of London A, pp 645-655
- 820 Kutiel H, Maheras P (1998) Variations in the temperature regime across the Mediterranean during
821 the last century and their relationship with circulation indices. *Theor Appl Climatol* 61:39–53
- 822 Kutiel H, Benaroch Y (2002) North Sea-Caspian Pattern (NCP)-An upper level atmospheric
823 teleconnection affecting the Eastern Mediterranean: Identification and definitions. *Theor Appl*
824 *Climatol* 71:17–28
- 825 Kutiel H, Maheras P, Türkeş M, Paz S (2002) North Sea – Caspian Pattern (NCP) – an upper level
826 atmospheric teleconnection affecting the eastern Mediterranean – implications on the regional
827 climate. *Theor Appl Climatol* 72:173–192
- 828 Kutiel H, Türkeş M (2005) New evidence about the role of the North Sea – Caspian Pattern (NCP) on
829 the temperature and precipitation regimes in continental central Turkey. *Geogr Ann A* 87:501–
830 513
- 831 Leavitt SW, Long A (1984) Sampling strategy for stable carbon isotope analysis of tree rings in pine.
832 *Nature* 301:145–147
- 833 Leuenberger M (2007) To what extent can ice core data contribute to the understanding of plant
834 ecological developments of the past? In: Dawson T, Siegwolf R (eds) *Stable Isotopes as Indicators*
835 *of Ecological Change*. Academic Press, London, pp 211–234
- 836 Leuenberger M, Siegenthaler U, Langway CC (1992) Carbon isotope composition of atmospheric CO₂
837 during the last ice-age from an Antarctic ice core. *Nature* 357:488–490
- 838 Loader NJ, Robertson I, Barker AC, Switsur VR, Waterhouse JS (1997) An improved technique for the
839 batch processing of small wholewood samples to α -cellulose. *Chem Geol* 136:313–317

- 840 Luterbacher J, Dietrich D, Xoplaki E, Grosjean M, Wanner H (2004) European seasonal and annual
841 temperature variability, trends, and extremes since 1500. *Science* 303:1499–1503
- 842 Maheras P, Kutiel H (1999) Spatial and temporal variations in the temperature regime in the
843 Mediterranean and their relationship with circulation during the last century. *Int J Climatol*
844 19:745–764
- 845 Maheras P, Patrikas I, Karacostas T, Anagnostopoulou C (2000) Automatic classification of circulation
846 types in Greece: methodology, description, frequency, variability and trend analysis. *Theor Appl*
847 *Climatol* 67:205–223
- 848 Mann ME, Zhang Z, Hughes MK, Bradley RS, Miller SK, Rutherford S, Ni F (2008) Proxy-based
849 reconstructions of hemispheric and global surface temperature variations over the past two
850 millennia. *Proc Nat Acad Sci USA* 105:13252–13257
- 851 McCarroll D, Loader NJ (2004) Stable isotopes in tree rings. *Quaternary Sci Revi* 23:771–801
- 852 McCarroll D, Gagen MH, Loader NJ, Robertson I, Anchukaitis KJ, Los S, Young GHF, Jalkanen R,
853 Kirchhefer AJ, Waterhouse JS (2009) Correction of tree ring stable carbon isotope chronologies for
854 changes in the carbon dioxide content of the atmosphere. *Geochim Cosmochim Ac* 73:1539–1547
- 855 Meko DM (1981) Applications of Box-Jenkins Methods of time-series analysis to reconstruction of
856 drought from tree rings, Ph.D. Dissertation, University of Arizona, Tucson, pp 149
- 857 Mitchell JM Jr, Dzerdzeevskii B, Flohn H, Hofmeyr WL, Lamb HH, Rao KN, Wallen CC (1966) Climate
858 change. Report of a working group of the Commission for Climatology, World Meteorological
859 Organization Technical Note 79, Geneva
- 860 Moberg A, Sonechkin DM, Holmgren K, Datsenko NM, Karlén W (2005) Highly variable Northern
861 Hemisphere Temperatures Reconstructed from Low- and High-Resolution Proxy Data. *Nature*
862 433:613–617
- 863 Naumann C (1893) *Vom Goldenen Horn zu den Quellen des Euphrat*: Munich, Leipzig
- 864 Panzac D (1985) *La Peste Dans l’empire Ottoman 1700-1850*. Editions Peeters, Louvain

- 865 Pozo-Vázquez D, Gámiz-Fortis SR, Tovar-Pescador J, Esteban-Parra MJ, Castro-Díez Y (2005) El Niño–
866 Southern Oscillation events and associated European winter precipitation anomalies. *Int J*
867 *Climatol* 25:17–31
- 868 Proedrou M, Theoharatos G, Cartalis C (1997) Variations and trends in annual and seasonal air
869 temperature in Greece determined from the ground and satellite measurements. *Theor Appl*
870 *Climatol* 57:65–78
- 871 Ribera P, Garcia R, Diaz HF, Gimeno L, Hernandez E (2000) Trends and interannual oscillations in the
872 main sea-level surface pressure patterns over the Mediterranean 1955–1990, *Geophys Res Lett*
873 27:1143–1146. doi:10.1029/1999GL010899
- 874 Rinn (2003) *TSAP-Win: Time Series Analysis and Presentation for Dendrochronology and Related*
875 *Applications*. Frank Rinn, Heidelberg, Germany
- 876 Roberts N (1998) *The Holocene: an environmental history*. Blackwell, Oxford
- 877 Rodwell MJ, Hoskins BJ (1996) Monsoons and the dynamics of deserts. *Q J Roy Meteor Soc*
878 122:1385–1404
- 879 Saji NH, Goswami BN, Vinayachandran PN, Yamagata T (1999) A dipole mode in the tropical Indian
880 Ocean. *Nature* 401:360–363
- 881 Saji, N.H. and T. Yamagata (2003): Possible impacts of Indian Ocean Dipole mode events on global
882 climate. *Climate Res* 25:151–169
- 883 Saurer M, Cherubini P, Bonani G, Siegwolf R (2003) Tracing carbon uptake from a natural CO₂ spring
884 into tree rings: an isotope approach. *Tree Physiol* 23:997–1004
- 885 Schönwiese CD (2008) *Klimatologie*. Ulmer, Stuttgart
- 886 Schubert BA, Jahren AH (2012) The effect of atmospheric CO₂ concentration on carbon isotope
887 fractionation in C₃ land plants. *Geochimica et Cosmochimica Acta* 96:29–43
- 888 Schweingruber FH (1983) *Der Jahrring. Standort, Methodik, Zeit und Klima in der Dendrochronologie*.
889 Paul Haupt, Bern

- 890 Sevgi O, Akkemik Ü (2007) A Dendroecological study on *Pinus nigra* Arn. on the different altitudes of
891 northern slopes of Kazdagları, Turkey. *Indian J Environ Biol* 28:73–75
- 892 Solanki SK, Usoskin IG, Kromer B, Schüssler M, Beer J (2004) An unusually active Sun during recent
893 decades compared to the previous 11,000 years. *Nature* 431:1084–1087
- 894 Telelis IG (2005) Historical-climatological information from the time of the Byzantine Empire (4th -
895 15th centuries AD). *Hist Meteor* 2:41–50
- 896 Telelis IG (2008) Climatic fluctuations in the Eastern Mediterranean and the Middle East AD 300-1500
897 from Byzantine documentary and proxy physical palaeoclimatic evidence - a comparison. *Jahrb*
898 *Österr Byzantinistik* 58:167–207
- 899 Thompson DWJ, Wallace JM (1998) The Arctic Oscillation signature in the wintertime geopotential
900 height and temperature fields. *Geophys Res Lett* 25:1297–1300
- 901 Touchan R, Garfin GM, Meko DM, Funkhouser G, Erkan N, Hughes MK, Wallin BS (2003) Preliminary
902 reconstructions of spring precipitation in southwestern Turkey from tree-ring width. *Int J Climatol*
903 23:157–171
- 904 Touchan R, Xoplaki E, Funkhouser G, Luterbacher J, Hughes MK, Erkan N, Akkemik U, Stephan J
905 (2005) Reconstruction of spring/summer precipitation for the Eastern Mediterranean from tree
906 ring widths and its connection to large-scale atmospheric circulation. *Climate Dyn* 25:75–98
- 907 Touchan R, Akkemik Ü, Hughes MK, Erkan N (2007) May-June precipitation reconstruction of
908 southwestern Anatolia, Turkey during the last 900 years from tree rings. *Quaternary Res* 68:196–
909 202
- 910 Treydte K, Schleser GH, Schweingruber FH, Winiger M (2001) The climatic significance of $\delta^{13}\text{C}$ in
911 subalpine spruces (Lötschental, Swiss Alps) - a case study with respect to altitude, exposure and
912 soil moisture. *Tellus* 53:593–611
- 913 Treydte K, Schleser GH, Helle G, Frank DC, Winiger M, Haug, GH, Esper J (2006) The twentieth century
914 was the wettest period in northern Pakistan over the past millennium. *Nature* 440:1179–1182
- 915 Troeng E, Linder S (1982) Gas exchange in a 20-year-old stand of Scots pine. *Physiol Plantarum* 54:7–
916 23

- 917 Türkeş M (1996) Spatial and temporal analysis of annual rainfall variations in Turkey. *Int J Climatol*
918 16:1057–1076
- 919 Türkeş M (1998) Influence of geopotential heights, cyclone frequency and Southern Oscillation on
920 rainfall variations in Turkey. *Int J Climatol* 18:649–680
- 921 Türkeş M, Sümer U, Kiliç G (1995) Variations and trends in annual mean air temperatures in Turkey
922 with respect to climatic variability. *Int J Climatol* 15:557–569
- 923 Türkeş M, Sümer UM, Kiliç G (2002) Persistence and periodicity in the precipitation series of Turkey
924 and associations with 500 hPa geopotential heights. *Climate Res* 21:59–81
- 925 Türkeş M, Sümer UM, Demir I (2002) Re-evaluation of trends and changes in mean, maximum and
926 minimum temperatures of Turkey for the period 1929–1999. *Int J Climatol* 22:947–977
- 927 Türkeş M, Erlat E (2003) Precipitation changes and variability in Turkey linked to the North Atlantic
928 oscillation during the period 1930–2000. *Int J Climatol* 23:1771–1796
- 929 Türkeş M, Erlat E (2008) Influence of the Arctic Oscillation on variability of winter mean temperatures
930 in Turkey. *Theor Appl Climatol* 92:75–85. doi:10.1007/s00704-007-0310-8
- 931 Türkeş M, Erlat E (2009) Winter mean temperature variability in Turkey associated with the North
932 Atlantic Oscillation. *Meteorol Atmos Phys* 105:211–225. doi:10.1007/s00703-009-0046-3
- 933 Turkish General Directorate of Meteorology (2008) Weather Station Databanks of Turkish General
934 Directorate of Meteorology, Ankara
- 935 van Oldenborgh GJ, Burgers G (2005) Searching for decadal variations in ENSO precipitation
936 teleconnections. *Geophys Res Lett* 32:L15701. doi:10.1029/2005GL023110
- 937 Voelker SL, Muzika R-M, Guyette, RP, Stambaugh MC (2006) Historical CO₂ growth enhancement
938 declines with age in *Quercus* and *Pinus*. *Ecol Monogr* 76:549–564
- 939 von Lürthe A (1991) Dendroökologische Untersuchungen an Kiefern und Eichen in den stadtnahen
940 Berliner Forsten. *Landschaftsentwicklung und Umweltforschung. Schriftenreihe des Fachbereichs*
941 *Landschaftsentwicklung der TU Berlin* 77, pp 186

- 942 Wahl ER, Anderson DM, Bauer BA, Buckner R, Gille EP, Gross WS, Hartman M, Shah A (2010) An
943 archive of high-resolution temperature reconstructions over the past 2+ millennia. *Geochem*
944 *Geophys Geosyst* 11:Q01001. doi:10.1029/2009GC002817
- 945 Wang D, Wang C, Yang X, Lu J (2005) Winter Northern Hemisphere surface air temperature variability
946 associated with the Arctic Oscillation and North Atlantic Oscillation. *Geophys Res Lett* 32:L16706.
947 doi:10.1029/2005GL022952
- 948 Werner A, Schönwiese C-D (2002) A statistical analysis of the North Atlantic Oscillation and its impact
949 on European temperature. *Global Atmosph Osc System* 8:293–306
- 950 Wigley TML, Briffa K, Jones PD (1984) On the average value of correlated time series, with
951 applications in dendroclimatology and hydrometeorology. *J Clim Appl Meteorol* 23:201–213
- 952 Wilson AT, Grinsted MJ (1977) $^{12}\text{C}/^{13}\text{C}$ in cellulose and lignin as palaeothermometers. *Nature*
953 265:133–135
- 954 Xoplaki E (2002) Climate variability over the Mediterranean. Ph.D. thesis, University of Bern, pp 193
955

956 List of Figures and Tables

957 **Fig. 1** Map with location of the sample site Jsibeli and climate diagram for the regional climate series
958 representing the mountainous inland region of SW Turkey, period 1949-2006 for temperature and 1931-2006 for
959 precipitation. The three stations, indicated by triangles, are located at similar elevations (Elmali 1113m asl,
960 Isparta 997m asl and Afyon 1034m asl (Turkish General Directorate of Meteorology 2008).

961 **Fig. 2** Plots of the Jsibeli raw tree-ring width series (A), raw $\delta^{13}\text{C}$ series (B), $\delta^{13}\text{C}$ corrected and z-transformed
962 series ($\delta^{13}\text{C}_{\text{CorZ}}$) (C) and sample depth for A to C (D) through time. The red graphs represent the means of the
963 raw and the corrected series.

964 **Fig. 3** Climate response plot for the Jsibeli site with the regional climate series (meteorological data from Elmali,
965 Isparta and Afyon): monthly coefficients of correlation for mean temperatures (black bars) and precipitation
966 sums (grey bars), significance levels are 0.05 (*), 0.01 (**), and 0.001 (***). Small letters on the left half of the
967 diagram cover the period January to December of the previous year and capital letters represent January to
968 December of the current year. Small letters a to d stand for annual values (current year) and the periods January-
969 to-March, January-to-May and July-to-September of the current season, respectively.

970 **Fig. 4** Reconstructed (solid line) and observed January-to-May temperature (dashed line) for calibration period
971 1978 to 2006 and verification period 1949 to 1977.

972 **Fig. 5** Reconstruction of January-to-May temperature based on $\delta^{13}\text{C}_{\text{CorZ}}$ with 95% confidence intervals (CI
973 calculated according to Chou 1972).

974 **Fig. 6** Comparison of trends in seasonal temperature data of composite record Elmali, Isparta and Afyon
975 (Winter: blue, Spring: green, Summer: red, Autumn: brown).

976 **Fig. 7** Correlations (1125-2006) between the Turkish January-to-May temperature reconstruction and two
977 hemispherical temperature reconstructions; high-, band-, and low-pass filtered (A, B, C) versions of Mann et al.
978 2008 (always left) and Moberg et al. 2005 (always right), significance levels are 0.05 (*), 0.01 (**), and 0.001
979 (***).

980 **Fig. 8** Comparison of the Turkish January-to-May temperature reconstruction and two hemispherical
981 temperature reconstructions (Mann et al. 2008, brown, and Moberg et al. 2005, green), 61-year moving averages.

982 **Fig. 9** Spatial field correlations (van Oldenborgh and Burgers, 2005) between mean Jan-May temperature and
 983 $\delta^{13}\text{C}_{\text{CorZ}}$ (1949-2006), upper map: old world overview, lower map: eastern Mediterranean, black star indicates
 984 location of the study site .

985 **Fig. 10** Spectral analysis of the Jan-May temperature reconstruction for the period 1125-2006 shows significant
 986 peaks at approximately 87, 54, 40, 32 and 26 years. 50, 90, 95, 99 and 99.9 % confidence levels are indicated.

987 **Fig. 11** Coefficients of correlation between Jan-May temperature reconstruction and Jan-May MOI (red), NCPI
 988 (blue) and EAWR (green) in moving windows of 13 years (95 % confidence levels are indicated); for
 989 comparison printed on top, the z-scores of the corresponding series (MOI red, NCPI blue, EAWR green and Jan-
 990 May temperature reconstruction in black, all smoothed with a 13-year mean).

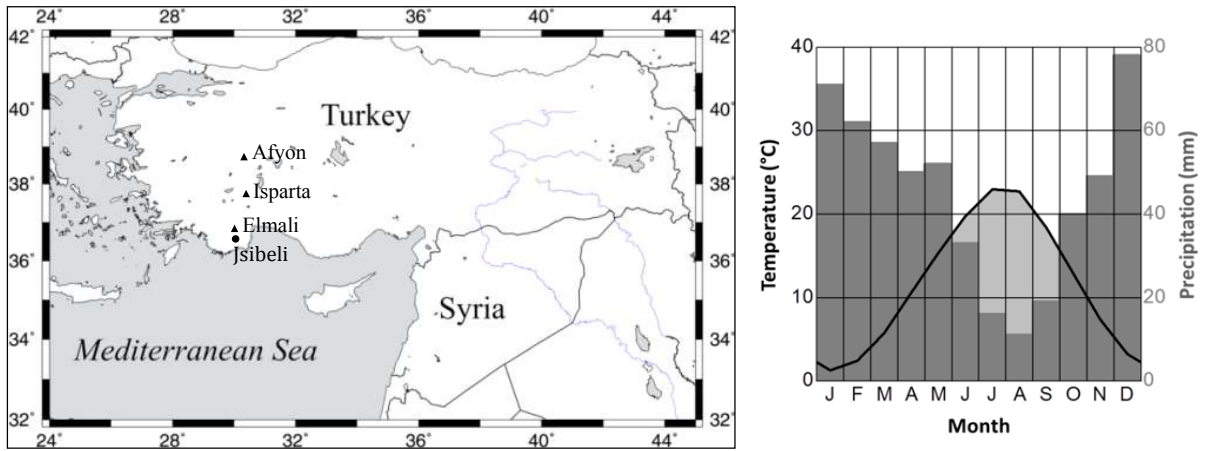
991 **Fig. 12** Coefficients of correlation between Jan-May temperature reconstruction and Jan-May NAO (red), AO
 992 (blue), NINO4 (brown) and DMI (orange) in moving windows of 13 years (95 % confidence levels are
 993 indicated); for comparison printed on top, the z-scores of the corresponding series (NAO red, AO blue, NINO4
 994 brown, DMI orange and Jan-May temperature reconstruction in black, all smoothed with a 13-year mean).

995 **Table 1** Reconstruction statistics for $\delta^{13}\text{C}_{\text{CorZ}}$

996 **Table 2** Comparison of correlations between the Jan-May temperature reconstruction and monthly to seasonal
 997 climate indices (NAO, AO, MOI, NCPI, EAWR, NINO4 and DMI) (small letters: months of previous year;
 998 capital letters: months of current year; confidence levels: 95%=bold; 99%=bold & underlined; 99.9%= bold,
 999 underlined & italics; the confidence intervals differ slightly due to selected time series lengths; 56 yrs: NAO,
 1000 AO, EAWR, NINO4; 50 yrs: MOI, DMI; 40 yrs: NCPI)

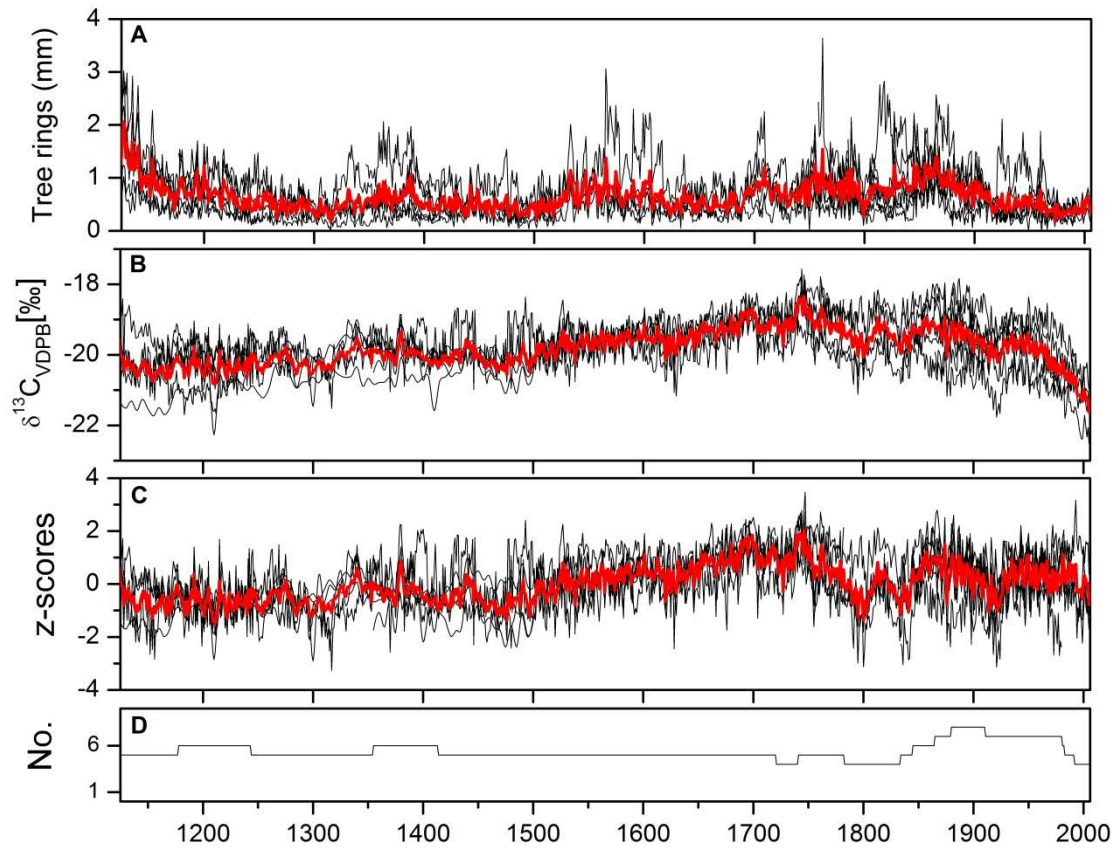
1001 **Figures and Tables**

1002



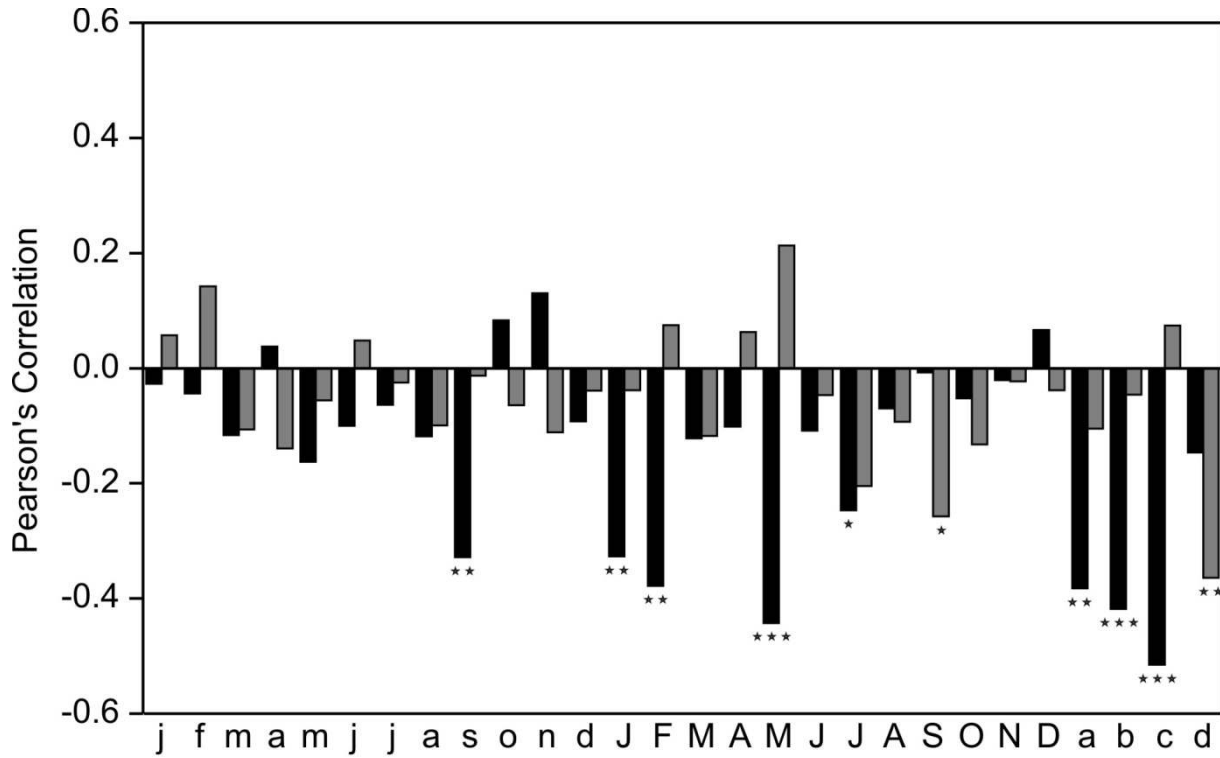
1003

1004 **Fig. 1** Map with location of the sample site Jsibeli and climate diagram for the regional climate series
 1005 representing the mountainous inland region of SW Turkey, period 1949-2006 for temperature and 1931-2006 for
 1006 precipitation. The three stations, indicated by triangles, are located at similar elevations (Elmalı 1113m asl,
 1007 Isparta 997m asl and Afyon 1034m asl (Turkish General Directorate of Meteorology 2008).



1008

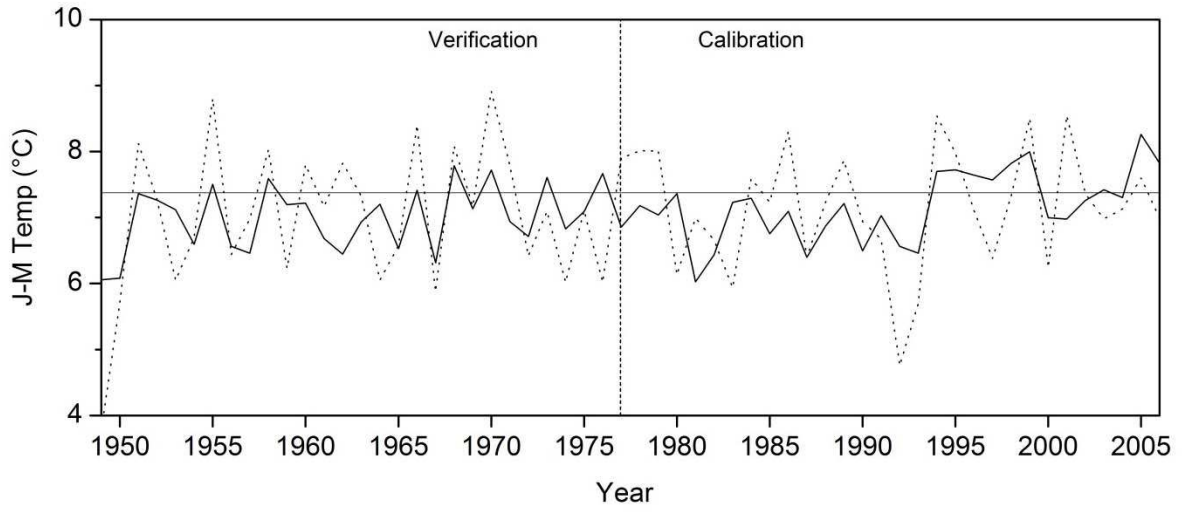
1009 **Fig. 2** Plots of the Jsibeli raw tree-ring width series (A), raw $\delta^{13}\text{C}$ series (B), $\delta^{13}\text{C}$ corrected and z-transformed
 1010 series ($\delta^{13}\text{C}_{\text{CorZ}}$) (C) and sample depth for A to C (D) through time. The red graphs represent the means of the
 1011 raw and the corrected series.



1012 **Fig. 3** Climate response plot for the Jsibeli site with the regional climate series (meteorological data from Elmali,
 1013 Isparta and Afyon): monthly coefficients of correlation for mean temperatures (black bars) and precipitation
 1014 sums (grey bars), significance levels are 0.05 (*), 0.01 (**), and 0.001 (***). Small letters on the left half of the
 1015 diagram cover the period January to December of the previous year and capital letters represent January to
 1016 December of the current year. Small letters a to d stand for annual values (current year) and the periods January-
 1017 to-March, January-to-May and July-to-September of the current season, respectively.

1019

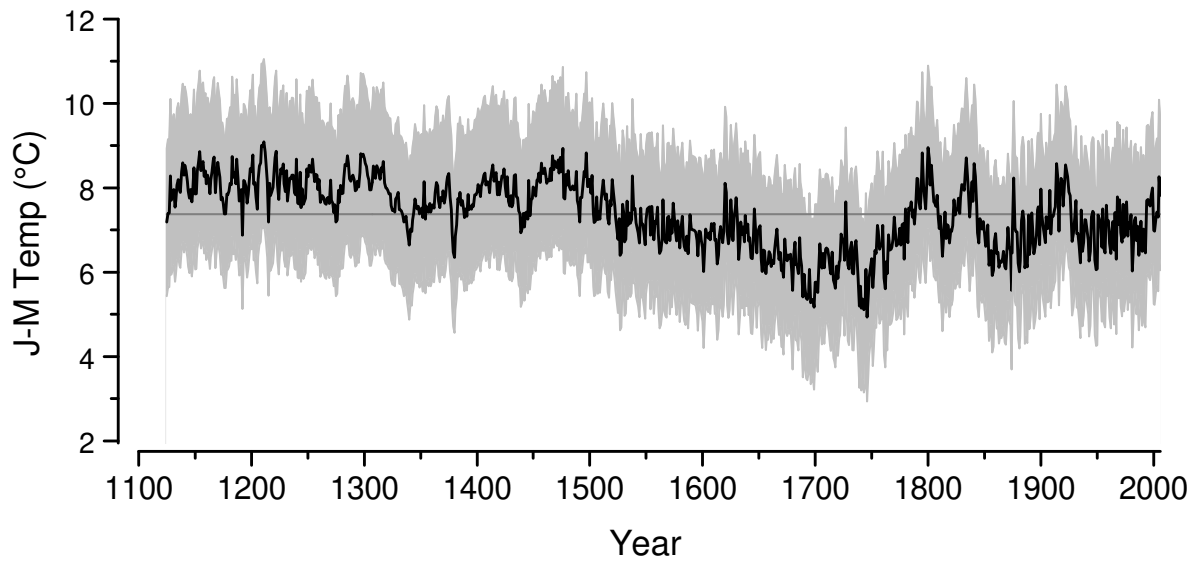
1020



1021

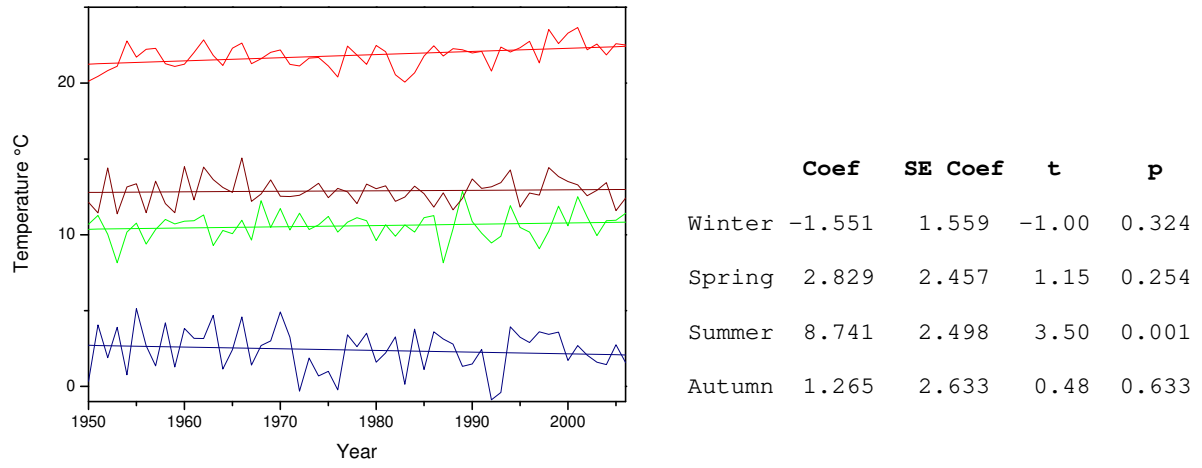
1022 **Fig. 4** Reconstructed (solid line) and observed January-to-May temperature (dashed line) for calibration period

1023 1978 to 2006 and verification period 1949 to 1977.

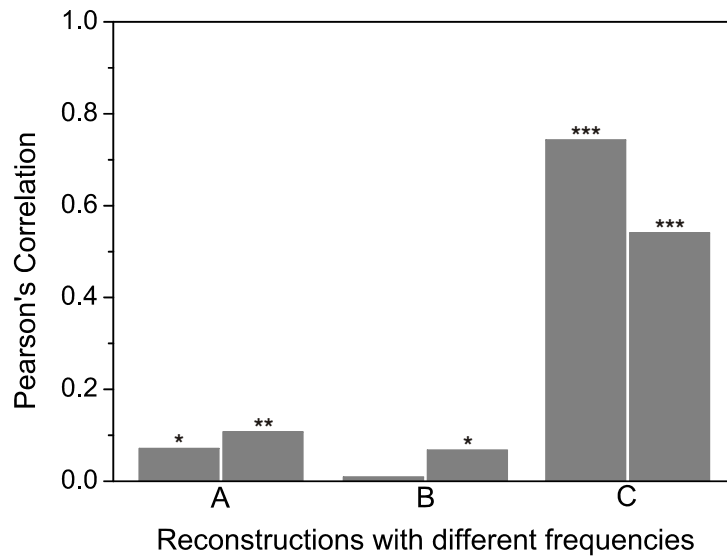


1024

1025 **Fig. 5** Reconstruction of January-to-May temperature based on $\delta^{13}\text{C}_{\text{CorZ}}$ with 95% confidence intervals (CI
1026 calculated according to Chou 1972).

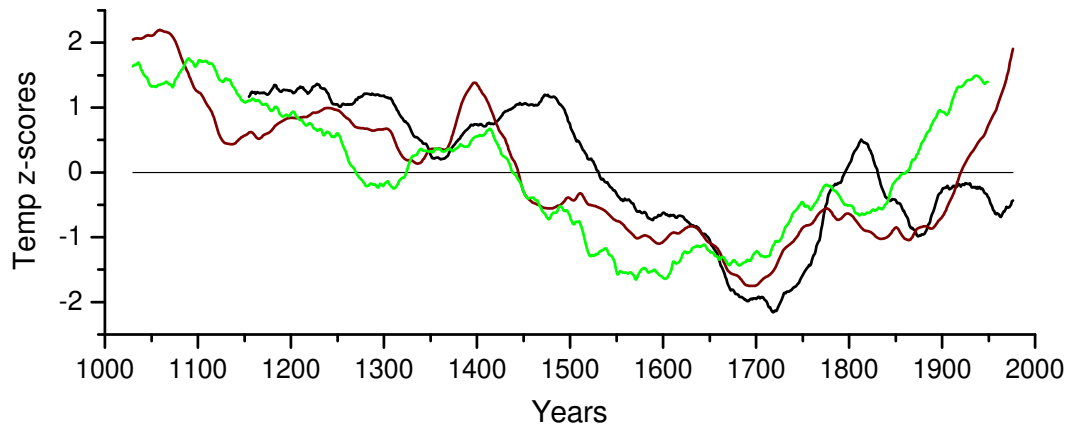


1027 **Fig. 6** Comparison of trends in seasonal temperature data of composite record Elmali, Isparta and Afyon
 1028 (Winter: blue, Spring: green, Summer: red, Autumn: brown).



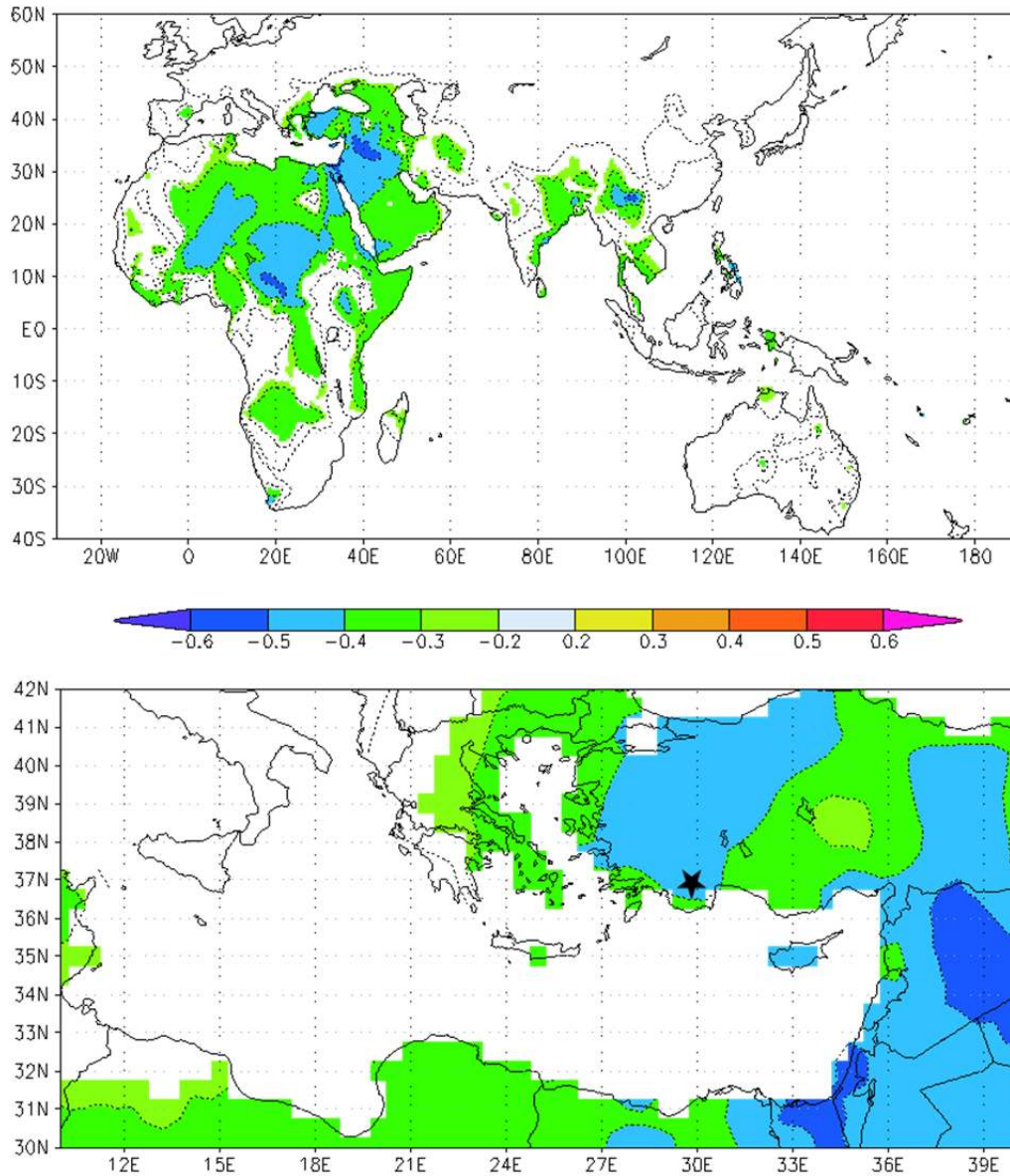
1029

1030 **Fig. 7** Correlations (1125-2006) between the Turkish January-to-May temperature reconstruction and two
1031 hemispherical temperature reconstructions; high-, band-, and low-pass filtered (A, B, C) versions of Mann et al.
1032 2008 (always left) and Moberg et al. 2005 (always right), significance levels are 0.05 (*), 0.01 (**), and 0.001
1033 (***).



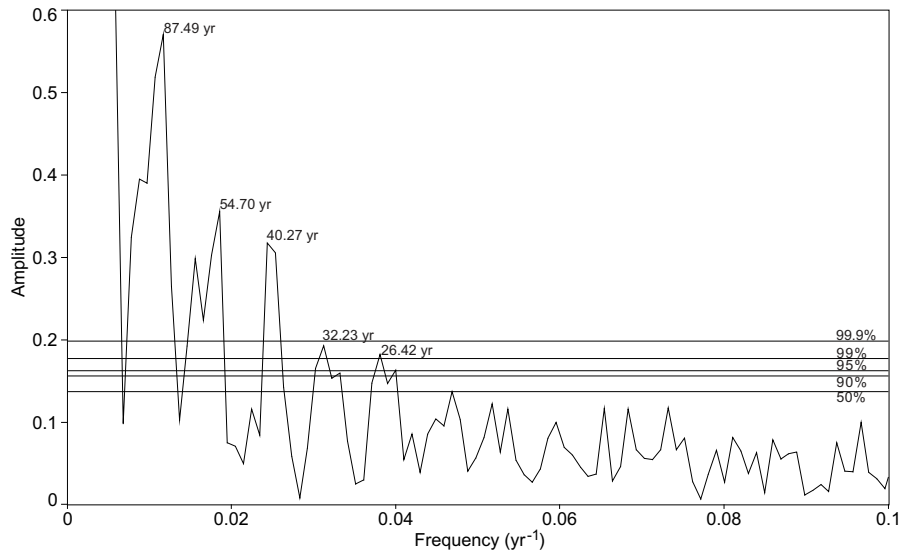
1034

1035 **Fig. 8** Comparison of the Turkish January-to-May temperature reconstruction and two hemispherical
1036 temperature reconstructions (Mann et al. 2008, brown, and Moberg et al. 2005, green), 61-year moving averages.



1037

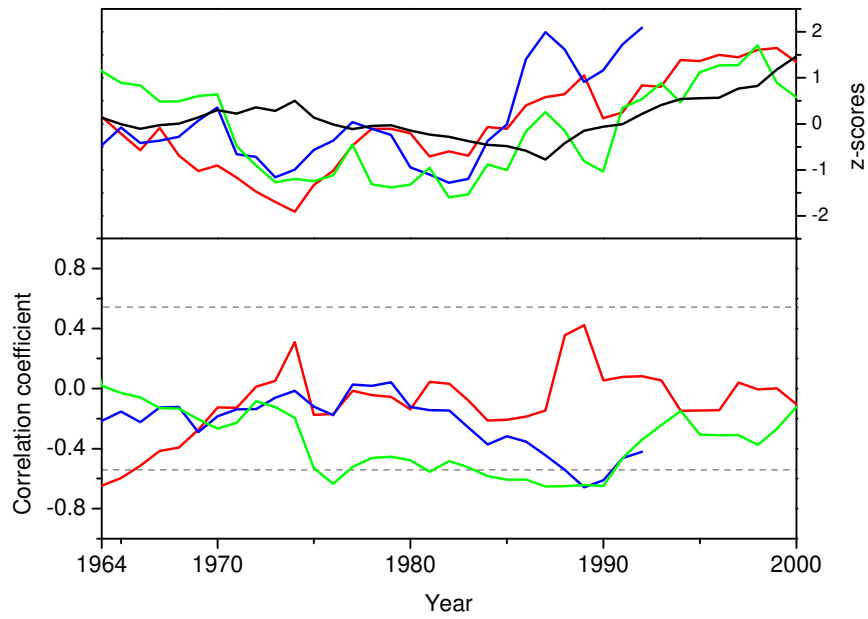
1038 **Fig. 9** Spatial field correlations (van Oldenborgh and Burgers, 2005) between mean Jan-May temperature and
 1039 $\delta^{13}\text{C}_{\text{CorZ}}$ (1949-2006), upper map: old world overview, lower map: eastern Mediterranean, black star indicates
 1040 location of the study site.



1041

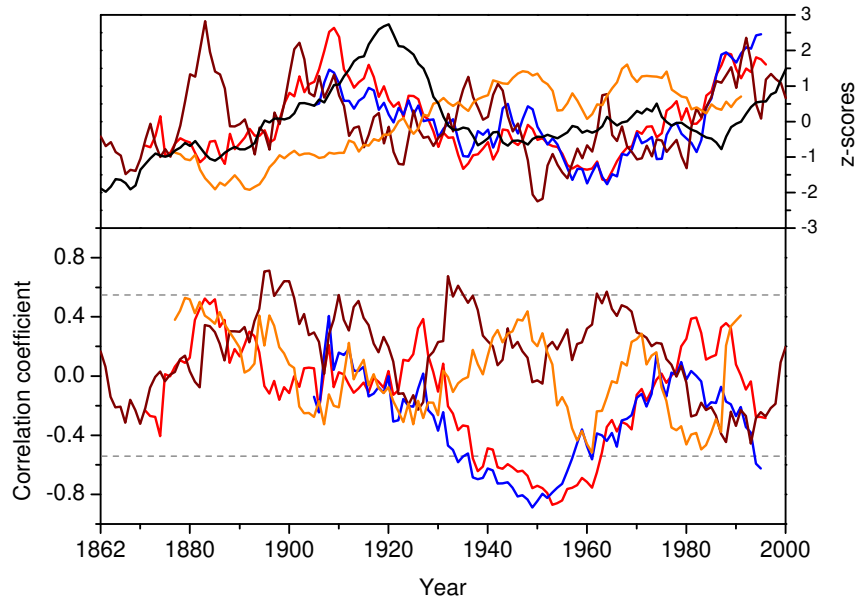
1042 **Fig. 10** Spectral analysis of the Jan-May temperature reconstruction for the period 1125-2006 shows significant

1043 peaks at approximately 87, 54, 40, 32 and 26 years. 50, 90, 95, 99 and 99.9 % confidence levels are indicated.



1044

1045 **Fig. 11** Coefficients of correlation between Jan-May temperature reconstruction and Jan-May MOI (red), NCPI
 1046 (blue) and EAWR (green) in moving windows of 13 years (95 % confidence levels are indicated); for
 1047 comparison printed on top, the z-scores of the corresponding series (MOI red, NCPI blue, EAWR green and Jan-
 1048 May temperature reconstruction in black, all smoothed with a 13-year mean).



1049

1050 **Fig. 12** Coefficients of correlation between Jan-May temperature reconstruction and Jan-May NAO (red), AO
 1051 (blue), NINO4 (brown) and DMI (orange) in moving windows of 13 years (95 % confidence levels are
 1052 indicated); for comparison printed on top, the z-scores of the corresponding series (NAO red, AO blue, NINO4
 1053 brown, DMI orange and Jan-May temperature reconstruction in black, all smoothed with a 13-year mean).

1054 **Table 1** Reconstruction statistics for $\delta^{13}\text{C}_{\text{corZ}}$

	$\delta^{13}\text{C}_{\text{corZ}}$
Full Rsq (2006-1949)	0.27
Rsqcal (2006-1978)	0.18
RsqVer (1977-1949)	0.37
RE	0.29
CE	0.28

1055

1056 **Table 2** Comparison of correlations between the Jan-May temperature reconstruction and monthly to seasonal
 1057 climate indices (NAO, AO, MOI, NCPI, EAWR, NINO4 and DMI) (small letters: months of previous year;
 1058 capital letters: months of current year; confidence levels: 95%=bold; 99%=bold & underlined; 99.9%= bold,
 1059 underlined & italics; the confidence intervals differ slightly due to selected time series lengths; 56 yrs: NAO,
 1060 AO, EAWR, NINO4; 50 yrs: MOI, DMI; 40 yrs: NCPI)

<i>Month/Season</i>	NAO	AO	MOI	NCPI	EAWR	NINO4	DMI
<i>jan</i>	0.00	0.04	0.01	-0.07	-0.01	0.18	0.02
<i>feb</i>	0.03	0.05	-0.16	0.04	0.19	0.18	-0.23
<i>mar</i>	0.04	0.11	0.11	0.04	-0.01	0.20	-0.05
<i>apr</i>	0.08	0.19	0.00	-0.11	-0.05	0.23	-0.14
<i>may</i>	-0.32	<u>-0.42</u>	0.14	<u>-0.37</u>	-0.14	0.28	0.22
<i>jun</i>	-0.12	-0.22	-0.16	0.01	0.30	0.25	0.28
<i>jul</i>	0.05	-0.06	0.04	0.32	0.00	0.22	0.18
<i>aug</i>	0.21	0.04	-0.33	0.13	-0.33	0.24	0.29
<i>sep</i>	-0.05	-0.04	-0.03	-0.11	-0.16	0.22	0.19
<i>oct</i>	0.04	0.02	-0.02	0.31	0.11	0.20	0.11
<i>nov</i>	-0.04	0.05	-0.10	0.04	0.03	0.18	-0.09
<i>dec</i>	0.02	0.07	-0.13	0.09	-0.02	0.17	0.01
<i>Jan</i>	-0.04	-0.13	-0.01	-0.02	-0.18	0.15	0.00
<i>Feb</i>	-0.01	-0.06	-0.10	-0.21	-0.02	0.12	0.16
<i>Mar</i>	0.02	-0.12	-0.07	-0.02	0.02	0.13	-0.02
<i>Apr</i>	-0.22	<u>-0.36</u>	0.07	-0.30	-0.01	0.09	-0.06
<i>May</i>	0.07	-0.06	-0.05	-0.02	-0.14	0.05	-0.04
<i>apr-may</i>				<u>-0.36</u>			
<i>apr-oct</i>						0.26	
<i>may-jun</i>	-0.31	<u>-0.42</u>				0.28	0.28
<i>may-aug</i>							0.29
<i>jun-aug</i>							
<i>jul-oct</i>				0.27			
<i>aug-sep</i>					-0.33		
<i>Feb-Apr</i>				-0.27			
<i>Mar-May</i>		-0.26					

1061